DO-TH 06/05
July 2006

On the transport equations of cosmic neutrinos passing through Earth and secondary ν_μ fluxes

S. Rakshit and E. Reya

Universität Dortmund, Institut für Physik,
D-44221 Dortmund, Germany

Abstract

The convergence of the iterative solutions of the transport equations of cosmic muon and tau neutrinos propagating through Earth is studied and analyzed. For achieving a fast convergence of the iterative solutions of the coupled transport equations of ν_τ, $\bar{\nu}_\tau$ and the associated $\tau^\pm$ fluxes, a new semi–analytic input algorithm is presented where the peculiar τ–decay contributions are implemented already in the initial zeroth order input. Furthermore, the common single transport equation for muon neutrinos is generalized by taking into account the contributions of secondary ν_μ and $\bar{\nu}_\mu$ fluxes due to the prompt τ–decay $\tau \to \nu_\mu$ initiated by the associated tau flux. Differential and total nadir angle integrated upward–going $\mu^- + \mu^+$ event rates are presented for underground neutrino telescopes and compared with the muon rates initiated by the primary ν_μ, ν_τ and τ fluxes.

1 Introduction

Upward–going cosmic neutrinos with energies below 10^8 GeV play a decisive role for underground neutrino telescopes, since the atmospheric background can be more effectively controlled, in contrast to downward–going cosmic neutrinos. While traversing through the Earth, upward–going muon (anti)neutrinos undergo attenuation (absorption) due to weak charged current (CC) and neutral current (NC) interactions as well as regeneration [1, 2] due to NC interactions. The latter shift the energy of the neutrinos, rather than absorbing them, to lower energies and populate the lower energy part of the initial cosmic neutrino flux spectra, thus adding to the naive non–regenerated $\mu^- + \mu^+$ event rates at the detector. Such propagation effects of muon (and electron) neutrinos through Earth are described by a single transport (integro–differential) equation which can be rather easily solved iteratively [1, 2, 3, 4, 5].

On the other hand tau (anti)neutrinos are not absorbed, but degraded in energy, in the Earth as long as the interaction length of the produced tau leptons is larger than their decay length (which holds for energies up to about 10^9 GeV). Because of these latter (semi)leptonic decays $\tau \to \nu_\tau X$, the Earth will not become opaque to ν_τ [6] since the τ^- produced in CC interactions decays back to ν_τ. This 'regeneration chain' $\nu_\tau \to \tau \to \nu_\tau \to \ldots$ continues until the ν_τ and $\bar{\nu}_\tau$, as well as the $\tau^\pm$ leptons, reach the detector on the opposite side of the Earth. Thus the propagation of high–energy tau neutrinos through the Earth is very different from muon and electron neutrinos, and we have now to deal with coupled transport equations for the $\overset{(-)}{\nu}_\tau$ and $\tau^\pm$ fluxes [4, 7, 8, 9, 10, 11, 12, 13]. Obtaining stable iterative solutions of these coupled integro–differential equations is far more involved as compared to the single transport equation for muon neutrinos. It is one of our main objectives to discuss the general qualitative and quantitative structure of these solutions and to present an efficient input algorithm which allows for a rather fast convergence of the iterative procedure. This applies to all present model cosmic

neutrino fluxes. Moreover the $\tau^- + \tau^+$ flux, generated by the initial cosmic $\nu_\tau + \bar{\nu}_\tau$ flux while traversing the Earth, gives rise to a secondary $\bar{\nu}_\mu + \nu_\mu$ flux [14] via $\tau \rightarrow \nu_\mu$ due to the prompt τ–decays like $\tau^- \rightarrow \nu_\tau \mu^- \bar{\nu}_\mu$. This adds considerable contributions to the primary cosmic $\nu_\mu + \bar{\nu}_\mu$ flux and may increase the $\mu^- + \mu^+$ rates at the detector site sizeably [9, 12], depending on the cosmic flux and nadir angle considered. Such effects require an extension of the simple single transport equation for $\overset{(-)}{\nu}_\mu$ and the inclusion of the appropriate prompt decay term reduces the convergence of the iterative procedure considerably.

The simple single transport equation for $\overset{(-)}{\nu}_\mu$ will be discussed for completeness in Sec. 2. Although frequently used, the excellent convergence of its iterative solutions has not been explicitly demonstrated thus far for more realistic cosmic neutrino fluxes, apart from some specific steep toy model neutrino fluxes [2]. In Sec. 3 we turn to the iterative solutions of the far more complicated coupled transport equations for $\overset{(-)}{\nu}_\tau$ and their associated $\tau^\pm$ fluxes. A new semi–analytic input algorithm is presented which allows for a fast convergence of the iterative solutions. The implications for the upward–going $\mu^- + \mu^+$ event rates for underground neutrino detectors for some relevant cosmic neutrino fluxes will be briefly outlined as well. The solutions of the generalized single transport equation for muon neutrinos, by taking into account the contributions of the secondary $\nu_\mu + \bar{\nu}_\mu$ flux from prompt $\tau^\pm$ decays based on the calculated associated $\tau^\pm$ fluxes, are discussed in Sec. 4. Their implications for the expected $\mu^- + \mu^+$ event rates, as initiated by various relevant cosmic neutrino model fluxes, are presented as well. Finally, our conclusions are summarized in Sec. 5.

2 The transport equation of muon neutrinos

Disregarding possible contributions from other neutrino flavors for the time being, the transport equation for upward–going cosmic muon (anti)neutrinos $\overset{(-)}{\nu}_\mu$ passing through

Earth can be written as [1, 2, 3, 4, 5]

$$\frac{\partial F_{\nu_\mu}(E,X)}{\partial X} = -\frac{F_{\nu_\mu}(E,X)}{\lambda_\nu(E)} + \frac{1}{\lambda_\nu(E)} \int_0^1 \frac{dy}{1-y}\, K_\nu^{\rm NC}(E,y)\, F_{\nu_\mu}(E_y,X) \tag{1}$$

where $F_{\nu_\mu} \equiv d\Phi_{\nu_\mu}/dE$ is the differential cosmic neutrino flux and $E_y = E/(1-y)$. The column depth $X = X(\theta)$, being the thickness of matter traversed by the upgoing leptons, depends on the nadir angle of the incident neutrino beam ($\theta = 0^{\rm o}$ corresponds to a beam traversing the diameter of the Earth); it is obtained from integrating the density $\rho(r)$ of the Earth along the neutrino beam path L' at a given θ, $X(\theta) = \int_0^L \rho(L')dL'$ with $L = 2R_\oplus \cos\theta$, $R_\oplus \simeq 6371$ km, denoting the position of the underground detector, and $X(\theta)$ can be found, for example, in Fig. 15 of [15] in units of g/cm^2 = cm we. Furthermore $\lambda_\nu^{-1} = N_A \sigma_{\nu N}^{\rm tot}$, $N_A = 6.022 \times 10^{23} g^{-1}$, is the inverse neutrino interaction length where $\sigma_{\nu N}^{\rm tot} = \sigma_{\nu N}^{\rm CC} + \sigma_{\nu N}^{\rm NC}$ and

$$K_\nu^{\rm NC}(E,y) = \frac{1}{\sigma_{\nu N}^{\rm tot}(E)}\, \frac{d\sigma_{\nu N}^{\rm NC}(E_y,y)}{dy}\,. \tag{2}$$

The various CC and NC $\overset{(-)}{\nu} N$ cross sections are calculated as in [5, 13], with the relevant details to be found in [16], utilizing the QCD inspired dynamical small–x predictions for parton distributions according to the radiative parton model [17]. Notice that conventionally fitted parton distributions at the relevant weak scale $Q^2 = M_W^2$ would require additional ad hoc assumptions (see, e.g., [15, 18]) for the necessary extrapolations into the yet unmeasured small Bjorken–x region $x < 10^{-3}$ ($x \simeq M_W^2/2m_N E$). The first term in (1) describes the attenuation (absorption) of neutrinos when penetrating through the Earth, and the second one their regeneration consisting of the degrading shift in their energy. For definiteness all formulae are given for an incoming neutrino beam, but similar expressions hold of course for antineutrinos.

Equation (1) can be efficiently solved by the ansatz [2]

$$F_{\nu_\mu}(E,X) = F_{\nu_\mu}^0(E) \exp\left[-\frac{X}{\Lambda_{\nu_\mu}(E,X)}\right] \tag{3}$$

with an effective absorption (interaction) length

$$\Lambda_{\nu_\mu}(E,X) = \frac{\lambda_\nu(E)}{1 - Z_{\nu_\mu}(E,X)} \tag{4}$$

and where $F^0_{\nu_\mu}(E) \equiv F_{\nu_\mu}(E, X=0)$ denotes the initial cosmic neutrino flux which reaches the Earth's surface. Depending on the assumed cosmic neutrino flux, the Z_ν–factor can take any non–negative values. Its physics interpretation and the consequences for the shadowing factor $S \equiv \exp\left[-X/\Lambda_\nu\right]$ in (3) are immediate: $Z_\nu < 1$ (the only case considered in [2] relevant for steeper, i.e., soft model fluxes) implies $\Lambda_\nu > \lambda_\nu > 0$ thus $S < 1$, i.e. the neutrino flux will be further attenuated since absorption plays the dominant role; for $Z_\nu = 1$, $\Lambda_\nu = \infty$, i.e. $S = 1$ which means that regeneration and absorption compensate each other; finally $Z_\nu > 1$ implies $\Lambda_\nu < 0$ and $S > 1$, and consequently the NC regeneration in (1) can even cause an enhancement of the neutrino spectrum with respect to the initial flux $F^0_{\nu_\mu}(E)$ for certain energies and depths X. Inserting (3) into (1) yields

$$Z_{\nu_\mu}(E,X) = \frac{1}{X}\int_0^X dX' \int_0^1 dy\, K^{\rm NC}_\nu(E,y)\, \eta_\nu\,(E,y)\, e^{-X' D_{\nu_\mu}(E,E_y,X')} \tag{5}$$

with $\eta_\nu(E,y) = F^0_{\nu_\mu}(E_y)/(1-y)F^0_{\nu_\mu}(E)$ and $D_{\nu_\mu}(E,E_y,X') = \Lambda^{-1}_{\nu_\mu}(E_y,X') - \Lambda^{-1}_{\nu_\mu}(E,X')$. Using an iteration algorithm to solve for $Z_{\nu_\mu}(E,X)$, one can formally rewrite the solution of (5) after the n–th iteration as

$$Z^{(n+1)}_{\nu_\mu}(E,X) = \frac{1}{X}\int_0^X dX' \int_0^1 dy\, K^{\rm NC}_\nu(E,y)\, \eta_\nu(E,y)\, e^{-X' D^{(n)}_{\nu_\mu}(E,E_y,X')} \tag{6}$$

where

$$D^{(n)}_{\nu_\mu}(E,E_y,X') = \frac{1 - Z^{(n)}_{\nu_\mu}(E_y,X')}{\lambda_\nu(E_y)} - \frac{1 - Z^{(n)}_{\nu_\mu}(E,X')}{\lambda_\nu(E)}\ . \tag{7}$$

The reason why this iteration is expected to converge very fast is as follows: the kernel $K^{\rm NC}_\nu$ peaks very strongly [2, 19] at $y = 0$ and $y = 1$, with the contribution at $y \simeq 1$ being, however, exponentially suppressed in (6); thus the main contribution to the integral over y in (6) comes from the region around $y \simeq 0$ where $D_{\nu_\mu}(E,E_y,X') \to 0$ as $y \to 0$. Therefore the iteration should be robust with respect to choosing the $n = 0$ approximation

[2]. The most simple input choice is $Z^{(0)}_{\nu_\mu}(E,X') = 0$ in (7). For this case the analytic X'–integration in (6) yields

$$Z^{(1)}_{\nu_\mu}(E,X) = \int_0^1 dy K^{\rm NC}_\nu(E,y)\,\eta_\nu(E,y)\,\frac{1-e^{-XD_\nu(E,E_y)}}{XD_\nu(E,E_y)} \tag{8}$$

with

$$D_\nu(E,E_y) \equiv D^{(0)}_{\nu_\mu}(E,E_y,X') = \frac{1}{\lambda_\nu(E_y)} - \frac{1}{\lambda_\nu(E)}\ . \tag{9}$$

With the $n=1$ solution in (8) at hand, it is now straightforward to obtain iterations in higher orders, for example, for $n=2$ by inserting (8) into (7) gives $Z^{(2)}_{\nu_\mu}$ in (6).

Representative cosmic neutrino fluxes of some hypothesized sources are displayed in Fig. 1 which we shall partly use for all our subsequent calculations. Recent diffuse neutrino flux upper limits of AMANDA [20, 21] are shown by the bars with arrows – the latter indicate the still allowed region. Although the huge flux from active galactic nuclei of Stecker and Salamon (AGN–SS) [22] has been already excluded, we shall use it merely as a theoretical playground due to its unique spectrum at lower energies where $F^0_{\nu_\mu}(E) \sim$ const. for $E \lesssim 10^5$ GeV. On the other hand the AGN–M95 flux [23] is still compatible (although slightly in conflict) with the AMANDA upper bound, as are the gamma ray burst (GRB–WB) [24] and topological defect (TD–SLBY) [25] fluxes. These latter three fluxes will be used for our 'realistic' model calculations. The TD–SLSC [26] and Z–burst [27] fluxes are shown just for illustration since they are too minute for being tested with upward–going event rates [5]. Note that the initial cosmic (anti)neutrino fluxes $F^0_{\nu,\bar\nu}(E)$ in (3) which reach the Earth's surface are given by $F^0_{\nu_\mu} = F^0_{\bar\nu_\mu} = F^0_{\nu_\tau} = F^0_{\bar\nu_\tau} = \frac{1}{4}d\Phi/dE$ with Φ being the cosmic $\nu_\mu + \bar\nu_\mu$ flux at the production site in Fig. 1.

For a better comparison of our quantitative results with the ones obtained in the literature, we also employ two generic initial fluxes incident on the surface of the Earth at a nadir angle $\theta = 0^{\rm o}$ of the form [4, 7]

$$F^0_{\nu_\mu+\bar\nu_\mu}(E) \;=\; N_1 E^{-1}(1+E/E_0)^{-2}, \quad E_0 = 10^8\ {\rm GeV} \tag{10}$$

$$F^0_{\nu_\mu+\bar\nu_\mu}(E) \;=\; N_2 E^{-2} \tag{11}$$

with adjustable normalization factors N_i, for example, $N_1 = \frac{1}{2} \times 10^{-13}/(\text{cm}^2 \text{ sr s})$ and $N_2 = \frac{1}{2} \times 10^{-7}$ GeV$/(\text{cm}^2$ sr s). Notice that the generic E^{-1} energy dependence is representative for the TD and Z–burst fluxes in Fig. 1 for $E \lesssim 10^7$ GeV; and also for the GRB–WB flux for $E \lesssim 10^5$ GeV. Furthermore the latter GRB–WB flux behaves like E^{-2} in (11) for $10^5 < E \lesssim 10^7$ GeV, where such a power spectrum with index -2 is typical for shock acceleration (see, e.g., [21]).

Our results for $Z^{(1)}_{\nu_\mu}$ and $Z^{(2)}_{\nu_\mu}$ are shown in Figs. 2 and 3 for two typical values of the nadir angle, $\theta = 0^o$ ($X = 1.1 \times 10^{10}$ cm we) and $\theta = 50^o$ ($X = 3.6 \times 10^9$ cm we). The iteration converges very fast since in general the maximum difference between $Z^{(1)}_{\nu_\mu}$ and $Z^{(2)}_{\nu_\mu}$ is less than about 5%, $|Z^{(2)}_{\nu_\mu}/Z^{(1)}_{\nu_\mu} - 1| < 0.05$, and moreover $|Z^{(3)}_{\nu_\mu}/Z^{(2)}_{\nu_\mu} - 1| < 0.005$. Thus the first $n = 1$ iteration is already sufficiently stable and suffices for *all* cosmic neutrino fluxes considered at present [19]. Notice that for larger θ (smaller X) the difference between $Z^{(2)}_{\nu_\mu}$ and $Z^{(1)}_{\nu_\mu}$ decreases and therefore the stability increases. The results for $Z_{\bar{\nu}_\mu}$ are similar but $Z_{\bar{\nu}_\mu} > Z_{\nu_\mu}$ for $E \lesssim 10^6$ GeV where $\lambda_{\bar{\nu}} > \lambda_\nu$. The resulting ν_μ and $\bar{\nu}_\mu$ fluxes follow from (3) and can be found in [4, 5, 7].

3 The transport equations of tau neutrinos and taus

Apart from the absorption (attenuation) due to $\sigma^{\text{tot}}_{\nu N}$ and regeneration due to $\sigma^{\text{NC}}_{\nu N}$ in (1), for upward–going cosmic tau (anti)neutrinos $\overset{(-)}{\nu}_\tau$, it is important to take into account the regeneration from the $\tau^\pm$ decays as well as the contributions from the CC tau interactions.

The tau neutrino and tau fluxes then satisfy the following coupled transport equations:

$$\frac{\partial F_{\nu_\tau}(E,X)}{\partial X} = -\frac{F_{\nu_\tau}(E,X)}{\lambda_\nu(E)} + \frac{1}{\lambda_\nu(E)}\int_0^1 \frac{dy}{1-y}\, K_\nu^{\rm NC}(E,y)\, F_{\nu_\tau}(E_y,X) + \int_0^1 \frac{dy}{1-y}\, K_\tau(E,y) F_\tau(E_y,X) \tag{12}$$

$$\frac{\partial F_\tau(E,X)}{\partial X} = -\frac{F_\tau(E,X)}{\hat\lambda(E)} + \frac{\partial\left[\gamma(E) F_\tau(E,X)\right]}{\partial E} + \frac{1}{\lambda_\nu(E)}\int_0^1 \frac{dy}{1-y}\, K_\nu^{\rm CC}(E,y)\, F_{\nu_\tau}(E_y,X) \tag{13}$$

where $F_{\nu_\tau} \equiv d\Phi_{\nu_\tau}/dE$ and $F_\tau \equiv d\Phi_\tau/dE$ are the differential energy spectra (fluxes) of tau (anti)neutrinos and tau leptons and the initial fluxes at the surface of the Earth ($X = 0$) being given by $F^0_{\nu_\tau}(E) = F^0_{\bar\nu_\tau}(E) = \frac{1}{4} d\Phi/dE$ with Φ being the $\nu_\mu + \bar\nu_\mu$ flux at the cosmic production site in Fig. 1. The cross section kernel $K_\nu^{\rm NC}$ is defined in (2) and a similar expression holds for $K_\nu^{\rm CC}$. Furthermore

$$K_\tau(E,y) = \frac{1}{\lambda_\tau(E)}\, K_\tau^{\rm CC}(E,y) + \frac{1}{\lambda_\tau^{\rm dec}(E)}\, K_\tau^{\rm dec}(E,y) \tag{14}$$

where

$$K_\tau^{\rm CC}(E,y) = \frac{1}{\sigma_{\tau N}^{\rm tot}(E)}\,\frac{d\sigma_{\tau N}^{\rm CC}(E_y,y)}{dy}, \qquad K_\tau^{\rm dec}(E,y) = \frac{1}{\Gamma_\tau^{\rm tot}(E)}\,\frac{d\Gamma_{\tau\to\nu_\tau X'}(E_y,y)}{dy}$$

and $\lambda_\tau^{-1} = N_A \sigma_{\tau N}^{\rm tot} = N_A(\sigma_{\tau N}^{\rm CC} + \sigma_{\tau N}^{\rm NC})$, and $\hat\lambda^{-1} = (\lambda_\tau^{\rm CC})^{-1} + (\lambda_\tau^{\rm dec})^{-1}$ with $(\lambda_\tau^{\rm CC})^{-1} = N_A \sigma_{\tau N}^{\rm CC}$ in (13). The decay length of the $\tau^\pm$ is $\lambda_\tau^{\rm dec}(E,X,\theta) = (E/m_\tau) c\tau_\tau \rho(X,\theta)$ with $m_\tau = 1.777$ GeV, $c\tau_\tau = 87.11$ μm and ρ denoting the Earth's density (see, e.g., [15]). Furthermore, since $1/\Gamma_\tau^{\rm tot}(E) = (E/m_\tau)\tau_\tau$, the τ–decay distribution in (14) becomes $K_\tau^{\rm dec}(E,y) = (1-y)\, dn(z)/dy$ with $z \equiv E_{\nu_\tau}/E_\tau = E/E_y = 1-y$ and [7, 28]

$$\frac{dn(z)}{dy} = \sum_i B_i \left[g_0^i(z) + P g_1^i(z)\right] \tag{15}$$

with the polarization $P = \pm 1$ of the decaying $\tau^\pm$. The $\tau \to \nu_\tau X'$ branching fractions B_i into the decay channel i and the functions $g^i_{0,1}(z)$ are given in Table I of [7]. The

decay channels i considered are $\tau \to \nu_\tau \mu \nu_\mu$, $\tau \to \nu_\tau \pi$, $\tau \to \nu_\tau \rho$, $\tau \to \nu_\tau a_1$ and $\tau \to \nu_\tau X$ which have branching fractions of 0.18, 0.11, 0.26, 0.13 and 0.13, respectively. The lepton energy–loss is treated continuously [29, 30, 31] by the term proportional to $\gamma(E)$ in (13). Alternatively, the average energy–loss can be treated separately (stochastically) [32, 33], i.e., not including the term proportional to $\gamma(E)$ in (13) but using instead $-dE/dX = \gamma(E) = \alpha + \beta E$. We shall compare these two approaches for taus and muons toward the end of this Section. The most general solution of Eqs. (12) and (13) has been presented in [10, 13], and in the context of atmospheric muons in [31]. For the time being, however, we disregard the γ-term in (13) since observable non–negligible upward–going event rates are obtained only for energies $E < 10^8$ GeV [7, 13] where the energy–loss of the taus can be neglected [10, 32, 33, 34, 35].

In the relevant energy region below 10^8 GeV, the tau–lepton interaction length is much larger than the decay length of the τ (see, e.g., [33] and below), $\lambda_\tau(E) \gg \lambda_\tau^{\rm dec}(E)$, i.e., $K_\tau \simeq K_\tau^{\rm dec}/\lambda_\tau^{\rm dec}$ in (14) and $\hat{\lambda}_\tau^{-1} \simeq (\lambda_\tau^{\rm dec})^{-1}$ in (13). Solving (12) and (13) with a similar ansatz as for muon neutrinos in (3), we write

$$F_{\nu_\tau}(E,X) = F^0_{\nu_\tau}(E) \exp\left[-\frac{X}{\Lambda_{\nu_\tau}(E,X)}\right] \tag{16}$$

with an effective interaction (absorption) length

$$\Lambda_{\nu_\tau}(E,X) = \frac{\lambda_\nu(E)}{1 - Z(E,X)} \tag{17}$$

where $Z = Z_{\nu_\tau} + Z_\tau$. Inserting (16) into (12) and (13) yields [4, 13]

$$Z_{\nu_\tau}(E,X) = \frac{1}{X}\int_0^X dX' \int_0^1 dy\, K_\nu^{\rm NC}(E,y)\, \eta_\nu(E,y)\, e^{-X' D_{\nu_\tau}(E,E_y,X')} \tag{18}$$

with η_ν as in (5) since $F^0_{\nu_\mu} = F^0_{\nu_\tau}$ and $D_{\nu_\tau}(E,E_y,X') = \Lambda^{-1}_{\nu_\tau}(E_y,X') - \Lambda^{-1}_{\nu_\tau}(E,X')$, and

$$Z_\tau(E,X) = \frac{\lambda_\nu(E)}{X}\int_0^X dX' \int_0^1 dy\, \frac{K_\tau^{\rm dec}(E,y)}{\lambda_\tau^{\rm dec}(E,X')}\, F_\tau(E_y,X')\, \frac{\eta_\nu(E,y)}{F^0_{\nu_\tau}(E_y)}\, e^{X'/\Lambda_{\nu_\tau}(E,X')} \tag{19}$$

where the obvious dependence of $\lambda_\tau^{\rm dec}$ on $\theta' = \theta(X')$ has been suppressed and

$$
\begin{aligned}
F_\tau(E_y, X') &= \frac{F^0_{\nu_\tau}(E_y)}{\lambda_\nu(E_y)} \int_0^{X'} dX'' \int_0^1 dy'\, K_\nu^{\rm CC}(E_y, y')\, \eta_\nu(E_y, y')\, e^{-X''/\Lambda_{\nu_\tau}(E_{yy'}, X'')} \\
&\quad \times \exp\left[- \int_{X''}^{X'} dX'''/\lambda_\tau^{\rm dec}(E_y, X''') \right]
\end{aligned}
\tag{20}
$$

with $E_{yy'} = E_y/(1-y') = E/(1-y)(1-y')$. Notice that the tau–flux F_τ is generated by the CC interactions of the initial $F^0_{\nu_\tau}$ flux and attenuated in addition due to its decay. In order to solve for $Z(E,X)$ iteratively as for the $\overset{(-)}{\nu}_\mu$ fluxes in the previous Section, one has to make a proper choice for the initial input. Due to the D_{ν_τ} function in the exponential in (18) with $D_{\nu_\tau} \to 0$ in the relevant $y \to 0$ region, the iterative result for $Z_{\nu_\tau}(E,X)$ is very robust with respect to the initial input choice, as discussed after (7). Therefore we use again $Z^{(0)}_{\nu_\tau}(E,X') = 0$ on the rhs of (18). In the case of $Z_\tau(E,X)$ in (19) there is, however, no equivalent exponential as in (18) and thus the convergence of the iterative procedure becomes sensitive to the input choice. It turns out that a convenient and efficient input choice can be obtained by implementing the peculiar E and X dependence as implied by the τ–decay contributions in (19) from the very beginning. This can be achieved by choosing a vanishing Z–factor on the rhs of Z_τ in (19), in which case the X'–integral can be performed analytically [36] and the input for the total Z–factor becomes [13]

$$
\begin{aligned}
Z^{(0)}(E,X) &= \frac{\lambda_\nu(E)}{\lambda_\tau^{\rm dec}(E,\theta)} \int_0^1 dy \int_0^1 dy'\, K_\tau^{\rm dec}(E,y)\, K_\nu^{\rm CC}(E_y, y')\, \lambda_\nu^{-1}(E_y)\, \eta_\nu(E,y)\, \eta_\nu(E_y, y') \\
&\quad \times \frac{1}{X D_{\nu\tau}(E_y, E_{yy'})} \left\{ \frac{1}{D_{\tau\nu}(E, E_y)} \left(1 - e^{-X D_{\tau\nu}(E, E_y)}\right) \right. \\
&\quad \left. - \frac{1}{D_\nu(E, E_{yy'})} \left(1 - e^{-X D_\nu(E, E_{yy'})}\right) \right\} \\
&\simeq \lambda_\nu(E) \int_0^1 \frac{dy}{1-y} \int_0^1 dy'\, K_\tau^{\rm dec}(E,y)\, K_\nu^{\rm CC}(E_y, y')\, \lambda_\nu^{-1}(E_y)\, \eta_\nu(E,y)\, \eta_\nu(E_y, y') \\
&\quad \times \frac{1}{X D_\nu(E, E_{yy'})} \left(1 - e^{-X D_\nu(E, E_{yy'})}\right)
\end{aligned}
\tag{21}
$$

where the last approximation is due to $\lambda_\tau^{\rm dec} \ll \lambda_\nu$ in the relevant energy region $E < 10^8$ GeV, i.e., $Z^{(0)}$ becomes practically independent of the decay length $\lambda_\tau^{\rm dec}$. Furthermore

$D_\nu(E,E_y)$ is given in (9), $D_{\nu\tau}(E,E_y) = 1/\lambda_\nu(E_y) - 1/\lambda_\tau^{\rm dec}(E,\theta)$ and $D_{\tau\nu}(E,E_y) = -D_{\nu\tau}(E_y,E)$. We have checked that this input guarantees, for all cosmic neutrino fluxes considered at present, a faster convergence of the iterations than choosing [4] the solution for the ν_μ flux as an input, $Z^{(0)} = Z^{(1)}_{\nu_\mu}$ with $Z^{(1)}_{\nu_\mu}$ given in (8). Moreover, choosing [10] a vanishing initial input, $Z^{(0)} = 0$, as was perfectly sufficient for the ν_μ fluxes, results in the worst, i.e., slowest convergence of the iterative procedure. One can now rewrite the solution for $Z(E,X)$ in (18) and (19) after the n–th iteration as [36]

$$\begin{aligned} Z^{(n+1)}(E,X) &= \frac{1}{X}\int_0^X dX' \int_0^1 dy\, K_\nu^{\rm NC}(E,y)\,\eta_\nu(E,y)\, e^{-X' D^{(n)}_{\nu_\tau}(E,E_y,X')} \\ &+ \frac{\lambda_\nu(E)}{\lambda_\tau^{\rm dec}(E,\theta)}\,\frac{1}{X}\int_0^X dX' \int_0^1 dy\, K_\tau^{\rm dec}(E,y)\,\eta_\nu(E,y)\lambda_\nu^{-1}(E_y) \\ &\times e^{-X'/\lambda_\tau^{\rm dec}(E_y,\theta)}\, e^{X'/\Lambda^{(n)}_{\nu_\tau}(E,X')} \int_0^{X'} dX'' \int_0^1 dy'\, K_\nu^{\rm CC}(E_y,y')\,\eta_\nu(E_y,y') \\ &\times e^{-X''/\Lambda^{(n)}_{\nu_\tau}(E_{yy'},X'')}\, e^{X''/\lambda_\tau^{\rm dec}(E_y,\theta)} \end{aligned} \tag{22}$$

where $\Lambda^{(n)}_{\nu_\tau}(E,X') = \lambda_\nu(E)/[1 - Z^{(n)}(E,X')]$, i.e.,

$$D^{(n)}_{\nu_\tau}(E,E_y,X') = \frac{1 - Z^{(n)}(E_y,X')}{\lambda_\nu(E_y)} - \frac{1 - Z^{(n)}(E,X')}{\lambda_\nu(E)}\ . \tag{23}$$

Accordingly, the iterations have to be started with our initial $n = 0$ input in (21). After having obtained the final convergent result for $Z^{(n+1)}$, the final ν_τ flux $F^{(n+1)}_{\nu_\tau}(E,X)$ follows from (16),

$$F^{(n+1)}_{\nu_\tau}(E,X) = F^0_{\nu_\tau}(E)\, e^{-X/\Lambda^{(n+1)}_{\nu_\tau}(E,X)}\ , \tag{24}$$

which in turn gives the τ–flux

$$F^{(n+1)}_{\tau}(E,X) = \frac{1}{\lambda_\nu(E)}\, e^{-X/\lambda_\tau^{\rm dec}(E,\theta)} \int_0^X dX' \int_0^1 \frac{dy}{1-y}\, K_\nu^{\rm CC}(E,y)\, F^{(n+1)}_{\nu_\tau}(E_y,X')\, e^{X'/\lambda_\tau^{\rm dec}(E,\theta)}\ . \tag{25}$$

Similar expressions hold for antineutrinos as well.

The iterative results for the total Z–factor in (17) are shown in Figs. 4 and 5 where the initial input $Z^{(0)}$, as given in (21), is displayed by the dotted curves. For the generic

initial E^{-1} and E^{-2} fluxes in (10) and (11) we also show in Fig. 4 the results after the third iteration, $Z^{(3)}$, in order to illustrate the rate of convergence as well as its dependence on the nadir angle $\theta = 0^o$ ($X = 1.1 \times 10^5$ km we) and $\theta = 50^o$ ($X = 3.6 \times 10^4$ km we). In general it turns out that already the second ($n = 2$) iteration yields sufficiently accurate results, $Z^{(2)}$, provided one uses as input $Z^{(0)}$ in (21) as implied by the τ–decay. This holds also for the rather hard initial E^{-1} flux in Fig. 4 and the AGN–SS flux in Fig. 5 which imply large Z–factors, $Z \gg 1$. This is so because the maximum difference between the results of the next $n = 3$ iteration $Z^{(3)}$ and $Z^{(2)}$ is less than about 5% for all relevant initial cosmic neutrino fluxes. An accuracy of less than about 5% is certainly sufficient in view of the uncertainties inherent to models of cosmic neutrino fluxes (cf. Fig. 1). Obviously the iterative convergence improves even more for larger values of θ, i.e., smaller depths X, as can be deduced from Fig. 4. It should be emphasized that, in contrast to the case of muon neutrinos in Sec. 2, the *first* $n = 1$ iterative results for $Z^{(1)}$ are *not* sufficiently accurate as can be seen from Figs. 4 and 5 by comparing the dashed curves ($Z^{(1)}$) with the solid ones ($Z^{(2)}$): in some cases (harder initial fluxes) $Z^{(2)}$ becomes larger than $Z^{(1)}$ by about 20%. The results for $\bar{\nu}_\tau$, $Z = Z_{\bar{\nu}_\tau} + Z_{\tau^+}$, are again similar but larger than for ν_τ, $Z = Z_{\nu_\tau} + Z_{\tau^-}$, for $E \lesssim 10^6$ GeV where $\lambda_{\bar{\nu}} > \lambda_\nu$. Inserting the various iterative solutions of Figs. 4 and 5 into (16) we obtain the ν_τ fluxes for a given n–th iteration, $F^{(n)}_{\nu_\tau}(E, X)$. The ratios of these fluxes for two consecutive iterations, $F^{(n+1)}_{\nu_\tau}/F^{(n)}_{\nu_\tau}$, are displayed in Figs. 6 and 7. Whereas the first iteration relative to the zeroth input, $F^{(1)}_{\nu_\tau}/F^{(0)}_{\nu_\tau}$, is way off the final result as shown by the dashed curves, the second iteration suffices already for obtaining a sufficiently accurate result as illustrated by $F^{(2)}_{\nu_\tau}/F^{(1)}_{\nu_\tau}$ by the solid curves. This is supported by the fact that an additional third iteration results in $|F^{(3)}_{\nu_\tau}/F^{(2)}_{\nu_\tau} - 1| < 0.05$ for all relevant initial cosmic neutrino fluxes considered. (This stability does *not* hold [7] for initial fluxes $F^0_{\nu_\mu+\bar{\nu}_\mu} \sim E^{-1}$ without an appropriate E^{-2} cutoff in (10) at very high energies, or for fluxes which are partly even flatter than E^{-1} up to highest energies like the Z–burst flux in Fig. 1. This instability is caused by the fact that $\eta_\nu(E, y) = 1$ for $F^0_\nu \sim E^{-1}$ in Z_τ in (19); thus the huge spike of $d\sigma^{\rm CC}_{\nu N}/dy$ at $y \to 1$ in (19) and (20) does

not get damped by powers of $(1-y)$ – as opposed to, e.g., $F^0_\nu \sim E^{-2}$ where $\eta_\nu = 1-y$. This, however, is of no concern for Z_{ν_μ} and Z_{ν_τ} in (5) and (18), respectively, since there the integrands are exponentially suppressed as $y \to 1$ via $\exp\left[-X' D_\nu(E, E_y, X)\right]$. Notice that the Z–burst flux is far too small for being tested with upward–going muon events [5, 13].) Therefore we consider $F^{(2)}_{\overset{(-)}{\nu}_\tau}(E, X)$ as our final result. It is furthermore obvious from Figs. 6 and 7 that the convergence of the iterative procedure strongly improves for increasing values of θ (decreasing X) as illustrated for $\theta = 50^o$.

The resulting total $\nu_\tau + \bar{\nu}_\tau$ fluxes for the various initial total cosmic fluxes $F^0_{\nu_\tau + \bar{\nu}_\tau}(E)$ are shown in Figs. 8 and 9 for three typical nadir angles $\theta = 0^o$ ($X = 1.1 \times 10^5$ km we), $\theta = 30^o$ ($X = 6.8 \times 10^4$ km we) and $\theta = 60^o$ ($X = 2.6 \times 10^4$ km we). The typical enhancement ('bump') of the attenuated and regenerated $\overset{(-)}{\nu}_\tau$ flux around 10^4 – 10^5 GeV at small values of θ, which is prominent for harder (flatter) initial fluxes like $F^0_{\overset{(-)}{\nu}_\tau} \sim E^{-1}$ in Fig. 8, and which is absent for $\overset{(-)}{\nu}_\mu$ fluxes, agrees with the original results of [4, 7, 9], as was also confirmed by a Monte Carlo simulation [34]. Such an enhancement is less pronounced for the GRB–WB and TD–SLBY fluxes in Fig. 9, and is absent for steeper fluxes like for the E^{-2} one in Fig. 8 and for the even steeper AGN–M95 flux in Fig. 9. Regeneration is responsible for an even more pronounced enhancement below 10^4 GeV for the AGN–SS flux in Fig. 9 since this flux is particularly hard below 10^5 GeV (cf. Fig. 1). This latter result is shown mainly for theoretical curiosity. From now on we shall disregard the cosmic AGN–SS flux since it is in serious conflict with recent experimental upper bounds [20, 21] as can be seen in Fig. 1. The results for the absolute total $\nu_\tau + \bar{\nu}_\tau$ and $\tau^- + \tau^+$ fluxes, arising from the initial cosmic $\nu_\tau + \bar{\nu}_\tau$ fluxes, are presented in Figs. 10 and 11. The $\nu_\tau + \bar{\nu}_\tau$ results correspond of course to the relative ratios shown in Figs. 8 and 9. Besides the generic initial fluxes in (10) and (11), we have in addition used only those initial cosmic fluxes in Fig. 1 which give rise to large enough upward–going $\mu^- + \mu^+$ event rates [5, 13] measurable in present and future experiments. Note that the $\tau^- + \tau^+$ fluxes in Figs. 10 and 11 at the detector site, despite being (superficially) suppressed with respect to the

$\nu_\tau + \bar{\nu}_\tau$ fluxes, sizeably contribute to the upward–going $\mu^- + \mu^+$ and shower event rates [13]. This is due to the fact that the τ fluxes do not require additional weak interactions for producing μ–events in contrast to the ν_τ fluxes. Because of the prompt $\tau^\pm$ decays, they furthermore give rise to a sizeable secondary $\bar{\nu}_\mu + \nu_\mu$ flux contribution to the original cosmic $\nu_\mu + \bar{\nu}_\mu$ flux, which will be discussed in Sec. 4.

In [13] a semi–analytic solution of the coupled transport equations (12) and (13) has been presented and used, which was obtained from the first $n = 1$ iteration starting with a vanishing input $Z^0(E, X) = 0$, instead of using (21). As we have seen, this approach does not provide sufficiently accurate results, despite opposite claims in the literature [10] (the first $n = 1$ iteration is sufficient only for very large values of θ close to 90^o, i.e., very small values of $X/\rho = \mathcal{O}(100$ km), relevant for neutrinos skimming the Earth's crust). This $n = 1$ iterative solution of [13] underestimates the correct results in some extreme cases (like for the hard initial E^{-1} flux at $\theta = 0^o$) by as much as 40%. On the other hand, for increasing values of θ this discrepancy disappears very quickly. Consequently, some of the *total* nadir–angle–integrated upward–going $\mu^- + \mu^+$ event rates calculated in [13] will be increased by less than about 2%. This is due to the fact that 80% of the $\mu^- + \mu^+$ rates are initiated by the $\nu_\mu + \bar{\nu}_\mu$ flux and only about 20% derives from the $\nu_\tau + \bar{\nu}_\tau$ and the associated $\tau^- + \tau^+$ fluxes. For completeness we present in Table 1 the correct expectations for the total $\mu^- + \mu^+$ event rates for the relevant dominant initial cosmic fluxes in Fig. 1, using Eqs. (12) and (14) of [13] for calculating the rates initiated by the $\nu_\tau + \bar{\nu}_\tau$ and $\tau^- + \tau^+$ fluxes, respectively.

Finally, it is also of interest to compare the tau–lepton range as given by our semi–analytic approach of treating the energy loss continuously in (13), with the one obtained by a stochastic treatment of the lepton energy loss (where the $\gamma(E)$ term in (13) is absent, i.e., the energy loss is treated separately, and the relevant survival probability $P(E, X)$ is calculated using Monte Carlo simulations, e.g., [32, 35, 37, 38]). To do this, we can drop the inhomogeneous neutrino term in (13) and the resulting homogeneous transport

equation for $F_\tau(E,X)$ can be easily solved [13]:

$$F_\tau(E,X) = F_\tau(\bar{E}(X,E),0)\exp\left[-\int_0^X A(\bar{E}(X',E))\,dX'\right] \tag{26}$$

with $A(E) \equiv 1/\hat{\lambda}(E) - \partial\gamma(E)/\partial E$, $\hat{\lambda}^{-1} \equiv (\lambda_\tau^{\rm CC})^{-1} + (\lambda_\tau^{\rm dec})^{-1}$, and where $d\bar{E}(X,E)/dX = \gamma(\bar{E})$ with $\bar{E}(0,E) = E$. The survival probability $P(E_0,X)$ for a tau–lepton with an initial energy E_0 at $X = 0$ is then defined by the ratio of the energy–integrated differential fluxes F_τ at X and $X = 0$: assuming, as usual, a monoenergetic initial flux in (26), $F_\tau(\bar{E}(X,E),0) \sim \delta(E - E_0)$, one obtains [10]

$$P(E_0,X) = \frac{\gamma(\tilde{E}_0)}{\gamma(E_0)}\,\exp\left[-\int_0^X A(\tilde{E}_0(X',E_0))\,dX'\right] \tag{27}$$

where we have used [13] $d\bar{E}/dE = \gamma(\bar{E})/\gamma(E)$ and $d\tilde{E}_0(X,E_0)/dX = -\gamma(\tilde{E}_0)$ with $\tilde{E}_0(0,E_0) = E_0$. The (tau) lepton range for an incident lepton energy E and a final energy $\tilde{E}(X,E)$ required to be greater than $E^{\rm min}$ at the detector, say, is then defined by

$$R(E) = \int_0^{X_{\rm max}} P(E,X)\,dX \tag{28}$$

where we have substituted E for E_0 in (27) and the upper limit of integration $X_{\rm max}$ derives from $\tilde{E}(X,E) \geq E^{\rm min}$. (Notice that for energy–independent values of α and β in $\gamma(E) = \alpha + \beta E$ one simply gets $X_{\rm max} = \frac{1}{\beta}\ln\frac{\alpha+\beta E}{\alpha+\beta E^{\rm min}}$.) For calculating the τ–lepton range $R_\tau(E)$ we use in γ_τ for the ionization energy loss [39, 40] $\alpha_\tau \simeq 2.0\times 10^{-3}$ GeV (cm we)$^{-1}$ and for the radiative energy loss (through bremsstrahlung, pair production and photonuclear interactions) [10] $\beta_\tau = \beta_\tau(E) \simeq [0.16 + 0.6(E/10^9\ {\rm GeV})^{0.2}]\times 10^{-6}$ (cm we)$^{-1}$ which parametrizes explicit model calculations [32, 35] for standard rock ($\rho = 2.65$ g/cm^3) reasonably well for $10^3 \lesssim E \lesssim 10^9$ GeV. Furthermore we impose [32] $E^{\rm min} = 50$ GeV. Our results for the τ–lepton range are shown in Fig. 12 which agree of course with the ones in [10]. The τ–decay term dictates the τ–range until $E > 10^7$ GeV where the tau–lepton energy loss becomes relevant. The dashed–dotted curve shows the range as obtained by omitting the contribution due to the CC interaction length $\lambda_\tau^{\rm CC}$ in $\hat{\lambda}$ in (27). This term will be relevant for $E \gtrsim 10^{10}$ GeV where $\lambda_\tau^{\rm CC}$ becomes comparable to $\lambda_\tau^{\rm dec}$ as

evident from Fig. 13. For comparison, stochastic Monte Carlo evaluations [32, 35, 38] of the τ–range are shown in Fig. 12 by the dotted curves which are of course strongly dependent on the assumed model extrapolations of the radiative cross sections to ultrahigh energies. Our results depend obviously also on such extrapolations due to specific choices of $\beta_\tau(E)$. Nevertheless, one concludes [10] from Fig. 12 that the *continuous* tau–lepton energy loss approach, as used in (13), yields very *similar* results as the stochastic Monte Carlo calculations where the energy loss is treated separately.

A similar conclusion holds for the muon–range $R_\mu(E)$ which we show for completeness in Fig. 14. Within the continuous muon energy loss approach, R_μ follows from (28) and (27) where the $\lambda_\tau^{\rm dec}$ term has to be omitted and in $\gamma_\mu(E) = \alpha_\mu + \beta_\mu E$ we take $\alpha_\mu \simeq \alpha_\tau \simeq 2.0 \times 10^{-3}$ GeV (cm we)$^{-1}$ and [32, 35] $\beta_\mu \simeq 6.0 \times 10^{-6}$ (cm we)$^{-1}$ which, moreover, reproduces best [5] the Monte Carlo result of Lipari and Stanev [37] for the average muon–range in standard rock for $E > 10^3$ GeV. Furthermore we choose [32] the final muon energy to be larger than $E^{\rm min} = 1$ GeV. (It should be noted that here $P_\mu(E, X) \simeq 1$ in (27), i.e., $R_\mu(E) \simeq X_{\rm max}$ in (28).) The muon–range R_μ calculated within the continuous muon energy loss approach yields again, as in the case of taus, very similar results as the stochastic Monte Carlo calculations [32, 35, 38] for $R_\mu^{\rm sto}$ as shown in Fig. 14. This is contrary to the conclusions reached in [10] that the continuous approach to the muon energy loss overestimates the muon–range as compared to stochastic Monte Carlo simulations. Therefore the continuous approach to the lepton energy loss is applicable to *both* taus and muons, since in both cases it yields similar results for the lepton ranges as the stochastic Monte Carlo simulations with the energy loss being treated separately.

4 The transport equation of muon neutrinos including secondary muon neutrinos from tau neutrino interactions

It has been pointed out [14] that the $\nu_\tau - \tau$ regeneration chain $\nu_\tau \to \tau \to \nu_\tau \to \ldots$ creates a secondary $\bar{\nu}_\mu + \nu_\mu$ flux due to the prompt, purely leptonic, tau decays $\tau^- \to \nu_\tau \mu^- \bar{\nu}_\mu$ and $\tau^+ \to \bar{\nu}_\tau \mu^+ \nu_\mu$. This will enhance the regenerated $\overset{(-)}{\nu}_\mu$ fluxes calculated according to (1) and thus also the 'naively' calculated [5, 15, 41] upward–going muon event rates at the detector site. Secondary neutrinos originate from the associated $\tau^\pm$ flux $F_\tau(E, X)$ and a prompt τ–decay like $\tau^- \to \bar{\nu}_\mu X'$. Adding those contributions, denoted by $G_{\overset{(-)}{\tau}^+ \to \overset{(-)}{\nu}_\mu}(E, X)$, to the simple transport equation (1) used thus far one obtains

$$\frac{\partial F_{\nu_\mu}(E,X)}{\partial X} = -\frac{F_{\nu_\mu}(E,X)}{\lambda_\nu(E)} + \frac{1}{\lambda_\nu(E)} \int_0^1 \frac{dy}{1-y} K_\nu^{\rm NC}(E,y)\, F_{\nu_\mu}(E_y, X) + G(E,X) \quad (29)$$

with $G = G_{\tau^+ \to \nu_\mu}$ where

$$G_{\tau^+ \to \nu_\mu}(E,X) = \frac{1}{\lambda_\tau^{\rm dec}(E,\theta)} \int_0^1 \frac{dy}{1-y} K_{\tau^+}^{\rm dec}(E,y)\, F_{\tau^+}(E_y, X) \quad (30)$$

and a similar transport equation holds for $F_{\bar{\nu}_\mu}$ with an appropriate expression for $G_{\tau^- \to \bar{\nu}_\mu}$. The relevant τ fluxes $F_{\tau^\pm}$ have been calculated in the previous Section (cf. Figs. 10 and 11). As in (14), the decay kernel in (30) is $K_{\tau^+}^{\rm dec}(E,y) = (1-y)\, dn_{\tau^+ \to \nu_\mu}(z)/dy$ with $z = 1 - y$ and the relevant $\tau^+ \to \nu_\mu X'$ decay distribution is given by [28]

$$\frac{dn_{\tau^+ \to \nu_\mu}(z)}{dz} = B_{\nu_\mu} \left[2 - 6z^2 + 4z^3 + P(-2 + 12z - 18z^2 + 8z^3)\right] \quad (31)$$

with $P = +1$ and the branching fraction $B_{\nu_\mu} = 0.18$. For a decaying $\tau^- \to \bar{\nu}_\mu X'$ one has $P = -1$ in (31). Notice that the $\overset{(-)}{\nu}_\mu$ spectrum in (31) is a little softer than the $\overset{(-)}{\nu}_\tau$ spectrum from the $\tau^\pm \to \overset{(-)}{\nu}_\tau X'$ decay [7, 28] in (15).

It should be noticed that the contribution of secondary neutrinos may alternatively be calculated using directly the $\overset{(-)}{\nu}_\tau$ fluxes $F_{\overset{(-)}{\nu}_\tau}(E,X)$ which give rise to the reaction

chains $\nu_\tau \xrightarrow{\rm CC} \tau^- \to \bar\nu_\mu X'$ and $\bar\nu_\tau \xrightarrow{\rm CC} \tau^+ \to \nu_\mu X'$. Denoting these contributions by $G_{\nu_\tau\to\bar\nu_\mu}(E,X)$ and $G_{\bar\nu_\tau\to\nu_\mu}(E,X)$, respectively, the inhomogeneous term in the transport equation (29) is given by $G = G_{\bar\nu_\tau\to\nu_\mu}$ with

$$G_{\bar\nu_\tau\to\nu_\mu}(E,X) = N_A \int_0^1 \frac{dy}{1-y} \int_0^1 \frac{dz}{z}\, \frac{dn_{\tau^+\to\nu_\mu}(z)}{dz}\, \frac{d\sigma^{\rm CC}_{\bar\nu N}(\frac{E_y}{z},y)}{dy}\, F_{\bar\nu_\tau}\left(\frac{E_y}{z},\, X\right) \qquad (32)$$

where $E_y/z = E/(1-y)z$, the decay distribution is given by (31) and the relevant flux $F_{\bar\nu_\tau}$ has been calculated in the previous Section (cf. Figs. 10 and 11). Although (32) and (30) yield the same quantitative results for $F_{\nu_\mu}(E,X)$, these two expressions should *not* be added since it would correspond to double–counting the effect of secondary neutrino production. This is due to the fact that the CC contribution $G_{\nu_\tau\to\tau}$ has been already included in (13) [third term on the rhs] for calculating F_τ. (The situation here is very similar to the calculation of the atmospheric muon flux [31, 28] where almost all muons come from meson decays with the meson flux being generated by nucleon interactions with air, i.e., by nucleon $\to$ meson transitions. These latter transitions are taken into account only in the evolution equation of the meson flux, but not anymore for the muon flux evolution.) For definiteness, we use the simpler expression in (30) for our subsequent calculations.

As in our previous cases, the most general transport equation (29) for muon neutrinos is easily solved by an ansatz like (16) for tau neutrinos,

$$F_{\nu_\mu}(E,X) = F^0_{\nu_\mu}(E) \exp\left[-\frac{X}{\Lambda_{\nu_\mu G}(E,X)}\right] \qquad (33)$$

with

$$\Lambda_{\nu_\mu G}(E,X) = \frac{\lambda_\nu(E)}{1 - Z_{\nu_\mu G}(E,X)} \qquad (34)$$

and $Z_{\nu_\mu G} = Z_{\nu_\mu} + Z_G$. Inserting (33) into (29) one obtains

$$Z_{\nu_\mu}(E,X) = \frac{1}{X}\int_0^X dX' \int dy\, K^{\rm NC}_\nu(E,y)\, \eta_\nu(E,y)\, e^{-X' D_{\nu_\mu}(E,E_y,X')} \qquad (35)$$

which is similar to (5) but with $D_{\nu_\mu}(E,E_y,X') = \Lambda^{-1}_{\nu_\mu G}(E_y,X') - \Lambda^{-1}_{\nu_\mu G}(E,X')$, and

$$Z_G(E,X) = \frac{\lambda_\nu(E)}{F^0_\nu(E)}\, \frac{1}{X} \int_0^X dX'\, G(E,X')\, e^{X'/\Lambda_{\nu_\mu G}(E,X')}\ . \qquad (36)$$

Using again an iteration algorithm to solve for $Z_{\nu_\mu G}(E,X)$, the solution of (35) and (36) after the n–th iteration becomes

$$Z^{(n+1)}_{\nu_\mu G}(E,X) = \frac{1}{X}\int_0^X dX' \int_0^1 dy\, K^{\rm NC}_\nu(E,y)\,\eta_\nu(E,y)\, e^{-X' D^{(n)}_{\nu_\mu}(E,E_y,X')} + \frac{\lambda_\nu(E)}{F^0_{\nu_\mu}(E)}\,\frac{1}{X}\int_0^X dX' G(E,X')\, e^{X'/\Lambda^{(n)}_{\nu_\mu G}}(E,X') \qquad (37)$$

where $D^{(n)}_{\nu_\mu}$ is as defined above with $\Lambda_{\nu_\mu G} \to \Lambda^{(n)}_{\nu_\mu G}$ and $\Lambda^{(n)}_{\nu_\mu G}(E,X') = \lambda_\nu(E)/\left[1 - Z^{(n)}_{\nu_\mu G}(E,X')\right]$. Due to the dominant and large τ–decay contribution $G(E,X)$ in (29), it turns out that the optimal input choice for providing sufficiently convergent iterative solutions is obtained by implementing, as in the case of tau neutrinos in Sec. 3, the peculiar E and X dependence as implied by the τ–decays, i.e., by G in (36) from the very beginning. Therefore we use again (see discussion after Eq. (20)) $Z^{(0)}_{\nu_\mu}(E,X) = 0$ and a vanishing Z–factor on the rhs of Z_G in (36) which gives for the total input Z–factor

$$Z^{(0)}_{\nu_\mu G}(E,X) = \frac{\lambda_\nu(E)}{F^0_\nu(E)}\,\frac{1}{X}\int_0^X dX'\, G(E,X')\, e^{X'/\lambda_\nu(E)}\ . \qquad (38)$$

Inserting this into the rhs of (37) results in the first iterative solution $Z^{(1)}_{\nu_\mu G}(E,X)$, and so on. In contrast to $Z^{(1)}_{\nu_\mu}$ in (8), $Z^{(1)}_{\nu_\mu G}$ does not provide us with a sufficiently accurate final result, i.e., the maximum difference between $Z^{(1)}_{\nu_\mu G}$ and $Z^{(2)}_{\nu_\mu G}$ is here *not* always less than about 5% for some initial cosmic neutrino fluxes and energies. Therefore we have to carry out one further iteration, as in the case of tau neutrinos in Sec. 3, by inserting $Z^{(1)}_{\nu_\mu G}$ into the rhs of (37) in order to obtain $Z^{(2)}_{\nu_\mu G}(E,X)$ which turns out to be sufficiently close to the final result since $|Z^{(3)}_{\nu_\mu G}/Z^{(2)}_{\nu_\mu G} - 1| \lesssim 0.02$.

Our iterative results for $Z^{(1,2)}_{\nu_\mu G}$ are shown in Figs. 15 and 16 together with the appropriate input $Z^{(0)}_{\nu_\mu G}$ in (38) shown by the dotted curves. In order to illustrate the faster iterative convergence for increasing θ (smaller X), the results for $\theta = 50^{\rm o}$ are presented in Fig. 15 as well. The sufficiently accurate results $Z^{(2)}_{\nu_\mu G}(E,X)$ and the similar expressions for $Z^{(2)}_{\bar\nu_\mu G}$, when inserted into (33), yield the final total fluxes $F_{\nu_\mu+\bar\nu_\mu}(E,X)$ shown in Figs. 17 and 18. The effect and importance of secondary neutrinos is best seen by

comparing our results (solid and dashed curves) with the usual ones [3, 5, 7, 15] obtained just for primary muon neutrinos ($G \equiv 0$ in (29)) shown by the dotted curves, which correspond of course to the results obtained in Sec. 2. Our results in Fig. 17 agree with the ones obtained in [9], within the approximations made there.

The corresponding $\overset{(-)}{\nu}_\mu$ initiated upward–going $\mu^{(+)}_-$ event rate per unit solid angle and second is calculated according to

$$N_{\mu^-}^{(\nu_\mu)} = N_A \int_{E_\mu^{\rm min}} dE_\nu \int_0^{1-E_\mu^{\rm min}/E_\nu} dy\, A(E_\mu)\, R_\mu(E_\mu, E_\mu^{\rm min}) \frac{d\sigma^{\rm CC}_{\nu_\mu N}(E_\nu, y)}{dy}\, F_{\nu_\mu}(E_\nu, X) \quad (39)$$

with $E_\mu = (1-y)E_\nu$ and the energy dependent area $A(E_\mu)$ of the considered underground detectors is taken as summarized in [5]. The muon–range is given by $R_\mu(E_\mu, E_\mu^{\rm min}) = \frac{1}{\beta_\mu} \ln \frac{\alpha_\mu + \beta_\mu E_\mu}{\alpha_\mu + \beta_\mu E_\mu^{\rm min}}$. It describes the range of an energetic muon being produced with energy E_μ and, as it passes through the Earth loses energy, arrives at the detector with energy above $E_\mu^{\rm min}$. The energy–loss parameters are taken as at the end of the previous Section, i.e., $\alpha_\mu = 2 \times 10^{-3}$ GeV (cm we)$^{-1}$ and $\beta_\mu = 6 \times 10^{-6}$ GeV (cm we)$^{-1}$. The integral over the neutrino energy E_ν was, for definiteness and better comparison [9], performed up to a maximum neutrino energy of 10^8 GeV. The differential θ–dependent $\mu^- + \mu^+$ rates for $E_\mu^{\rm min} = 10^4$ GeV and $E_\mu^{\rm min} = 10^5$ GeV are shown in Figs. 19 and 20. We also include the contributions initiated by the primary $\nu_\mu + \bar\nu_\mu$ flux, for brevity denoted by $\nu_\mu \to \mu$, and by the $\nu_\tau + \bar\nu_\tau$ flux via $\nu_\tau \to \tau \to \mu$ and the $\tau^- + \tau^+$ flux via $\tau \to \mu$ as discussed in the previous Section. The secondary neutrino contributions to the muon event rates have their largest relative contributions obviously at small nadir angles, with an enhancement over the primary $\nu_\mu + \nu_\tau + \tau$ initiated rates of up to 40% for the hard E^{-1}, AGN–M95 and TD–SLBY initial fluxes.

At small nadir angles, however, the event rates are smallest and statistics are low. For $\theta \gtrsim 60^{\rm o}$ the event rates are roughly a factor of (more than) 10 larger and the enhancement of the overall $\nu_\mu + \nu_\tau + \tau$ initiated muon rates (dashed–dotted curves in Figs. 19 and 20) can not be larger than about 15%. These results are more explicitly illustrated in Tables

2 and 3 where we present, besides the total nadir–angle–integrated rates, also the ones integrated over three typical θ–intervals. (Remember that this amounts to integrating (39) over $\int_0^{2\pi} d\varphi \int_{\theta_{\min}}^{\theta_{\max}} d\theta \sin\theta = 2\pi \int_{\theta_{\min}}^{\theta_{\max}} d\theta \sin\theta$, with $\theta_{\min} = 0^{\rm o}$ and $\theta_{\max} = 90^{\rm o}$ for the total rates.) Since secondary muon neutrinos contribute significantly to a muon excess only at small and medium nadir angles, $\theta < 60^{\rm o}$, the primary event rates (shown in brackets in Tables 2 and 3) can be enhanced by more than 20%, in particular for $E_\mu^{\min} = 10^5$ GeV. The statistics, however, are low since the fluxes are already strongly attenuated for $\theta < 60^{\rm o}$ (large X), cf. Figs. 17 and 18. On the other hand, most of the events are generated at large θ, $\theta > 60^{\rm o}$, where the effect of secondary neutrinos is sizeably reduced (cf. Figs. 19 and 20), the total rates in Tables 2 and 3 are increased by less than 10%. Since the expected angular resolution of present and proposed detectors [21, 42] is typically about $1^{\rm o}/(E_\nu/{\rm TeV})^{0.7}$, differential θ–dependent measurements should be feasible, in order to delineate experimentally the effects of secondary neutrino fluxes. Keeping in mind that the lifetime of the planned experiments is roughly ten years, it appears to be not unreasonable that the tenfold rates implied by Tables 2 and 3 may be observable in the not too distant future.

5 Summary and Conclusions

For the sake of completeness we have first studied the solutions of the single transport equation for cosmic $\overset{(-)}{\nu}_\mu$ neutrinos propagating through the Earth. Although frequently used, the excellent convergence of its iterative solutions has not been explicitly demonstrated thus far for more realistic and hard cosmic neutrino fluxes. Using the symbolic ansatz for the solution $F_\nu(E,X) = F_\nu^0(E) \exp\left[(1-Z)X/\lambda_\nu\right]$, with λ_ν being the neutrino interaction length, the most simple input choice $Z_{\nu_\mu}^{(0)}(E,X) = 0$ suffices to produce a sufficiently accurate iterative result $Z_{\nu_\mu}^{(1)}$ already after the first iteration, for all presently used initial cosmic model fluxes F_ν^0.

Turning to the iterative solutions of the far more complicated coupled transport equations for $\overset{(-)}{\nu}_\tau$ and their associated $\tau^\pm$ fluxes, a new semi–analytic input algorithm is presented which allows for a fast convergence of the iterative solutions: already a second $n = 2$ iteration suffices for obtaining a sufficiently accurate result $Z^{(2)}$ and thus for the final $F_{\overset{(-)}{\nu}_\tau}$ and its associated $F_{\tau^\pm}$ fluxes. In order to achieve this one has to implement the peculiar E and X dependence as implied by the $\tau^\pm$ decay contributions already into the initial zeroth order input $Z^{(0)}(E, X)$. Choosing a vanishing input $Z^{(0)} = 0$ as in the case for $\overset{(-)}{\nu}_\mu$ fluxes or even the final solution for the $\overset{(-)}{\nu}_\mu$ flux as an input, $Z^{(0)} = Z^{(1)}_{\nu_\mu}$, as frequently done, results in a far slower convergence of the iterative procedure. For completeness we briefly outline also the implications for the upward–going $\mu^- + \mu^+$ event rates for underground neutrino detectors using some relevant cosmic neutrino fluxes. These events are generated by the so called 'primary' $\overset{(-)}{\nu}_\mu$, $\overset{(-)}{\nu}_\tau$ and $\tau^\pm$ fluxes via the weak transitions and decays $\nu_\mu \overset{\text{CC}}{\to} \mu$, $\nu_\tau \overset{\text{CC}}{\to} \tau \to \mu$ and $\tau \to \mu$. Furthermore, for calculating the range $R_\tau(E)$ of tau–leptons, their energy loss can either be treated 'continuously' by including it directly in the transport equation, or 'stochastically' by treating it separately. Both approaches give very similar results for R_τ up to highest energies of 10^{12} GeV relevant at present. A similar agreement is obtained for the muon range $R_\mu(E)$. Therefore the continuous approach is applicable to both taus and muons. This is contrary to claims in the literature that the continuous approach overestimates R_μ as compared to stochastic Monte Carlo simulations.

Finally, we generalized the single transport equation for $\overset{(-)}{\nu}_\mu$, by taking into account the contributions of secondary ν_μ and $\bar{\nu}_\mu$ fluxes. These so called 'secondary' muon neutrino fluxes originate from prompt $\tau^\pm$ decays where the τ–leptons are generated by the regeneration chain $\nu_\tau \to \tau \to \nu_\tau \to \ldots$ when a cosmic ν_τ passes through the Earth. Thus the secondary $\nu_\mu + \bar{\nu}_\mu$ flux arises from the associated $\tau^\pm$ flux, as obtained from the coupled transport equations for ν_τ and τ, which initiates the $\tau \to \nu_\mu$ transitions ($\tau^- \to \nu_\tau \mu^- \bar{\nu}_\mu$ and $\tau^+ \to \bar{\nu}_\tau \mu^+ \nu_\mu$). In order to achieve a sufficiently fast convergence of the iterative

solutions of the single generalized transport equation of muon neutrinos, one again has to implement the peculiar E and X dependence as implied by the weak τ–decays already into the initial zeroth order input $Z^{(0)}(E,X)$. In this case one needs only $n = 2$ iterations for obtaining a sufficiently accurate result $Z^{(2)}(E,X)$ for calculating the final secondary ν_μ and $\bar{\nu}_\mu$ fluxes. The $\mu^- + \mu^+$ event rates initiated by the secondary neutrinos are largest obviously at small nadir angles ($\theta < 60^o$), with a relative enhancement of at most 40% over the primary $\nu_\mu + \nu_\tau + \tau$ initiated rates for the hard initial cosmic fluxes like AGN–M95 and TD–SLBY. At larger nadir angles, $\theta \gtrsim 60^o$, the muon rates are dominantly initiated by the primary $\nu_\mu + \nu_\tau + \tau$ flux and the secondary $\nu_\mu + \bar{\nu}_\mu$ flux becomes naturally less relevant. Thus the secondary neutrino flux will enhance the total nadir–angle–integrated muon event rates only by less than 10%. Nevertheless, it should be possible to observe the effects of secondary neutrinos with differential θ–dependent measurements, keeping in mind that the angular resolutions of the proposed underground neutrino telescopes will reach sub–arc–minute precisions.

Acknowledgements

We are grateful to W. Rhode for helpful discussions, in particular about lepton ranges, and for providing us with the results of the τ–ranges of the Chirkin–Rhode Monte Carlo calculations extended up to 10^{12} GeV. Similarly, we thank M.H. Reno for sending us her Monte Carlo results for the τ–range for energies up to 10^{12} GeV. This work has been supported in part by the 'Bundesministerium für Bildung und Forschung', Berlin/Bonn.

References

[1] A. Nicolaidis and T. Taramopoulos, *Phys. Lett.* **B386**, 211 (1996).

[2] V.A. Naumov and L. Perrone, *Astropart. Phys.* **10**, 239 (1999).

[3] J. Kwiecinski, A.D. Martin, and A.M. Stasto, *Phys. Rev.* **D59**, 093002 (1999).

[4] S. Iyer, M.H. Reno, and I. Sarcevic, *Phys. Rev.* **D61**, 053003 (2000).

[5] K. Giesel, J.-H. Jureit, and E. Reya, *Astropart. Phys.* **20**, 335 (2003).

[6] F. Halzen and D. Saltzberg, *Phys. Rev. Lett.* **81**, 4305 (1998).

[7] S. Iyer Dutta, M.H. Reno, and I. Sarcevic, *Phys. Rev.* **D62**, 123001 (2000).

[8] C. Hettlage and K. Mannheim, *Nucl. Phys. B* (Proc. Suppl.) **95**, 165 (2001).

[9] S. Iyer Dutta, M.H. Reno, and I. Sarcevic, *Phys. Rev.* **D66**, 077302 (2002).

[10] J.J. Tseng et al., *Phys. Rev.* **D68**, 063003 (2003).

[11] S. Hussain and D.W. McKay, *Phys. Rev.* **D69**, 085004 (2004).

[12] S. Yoshida, R. Ishibashi, and H. Miyamoto, *Phys. Rev.* **D69**, 103004 (2004).

[13] E. Reya and J. Rödiger, *Phys. Rev.* **D72**, 053004 (2005).

[14] J.F. Beacom, P. Crotty, and E.W. Kolb, *Phys. Rev.* **D66**, 021302(R) (2002).

[15] R. Gandhi, C. Quigg, M.H. Reno, and I. Sarcevic, *Astropart. Phys.* **5**, 81 (1996).

[16] M. Glück, S. Kretzer, and E. Reya, *Astropart. Phys.* **11**, 327 (1999).

[17] M. Glück, E. Reya, and A. Vogt, *Eur. Phys. J.* **C5**, 461 (1998).

[18] G.M. Frichter, D.W. McKay, and J.P. Ralston *Phys. Rev. Lett.* **74**, 1508 (1995); **77**, 4107 (1996) (E).

[19] K. Giesel, Master Thesis, University of Dortmund, 2003.

[20] K. Ackermann et al., (AMANDA Collaboration), *Astropart. Phys.* **22**, 339 (2005); K. Achterberg et al. (IceCube Collaboration), Proceedings of the 29th Intern. Cosmic Ray Conference, Pune, India, 2005 (astro–ph/0509330).

[21] F. Halzen, *Eur. Phys. J.* **C46**, 669 (2006).

[22] F.W. Stecker and M. Salamon, *Space Sci. Rev.* **75**, 341 (1996).

[23] K. Mannheim, *Astropart. Phys.* **3**, 295 (1995).

[24] E. Waxman and J.N. Bahcall, *Phys. Rev.* **D59**, 023002 (1999).

[25] G. Sigl, S. Lee, P. Bhattacharjee, and S. Yoshida, *Phys. Rev.* **D59**, 043504 (1999).

[26] G. Sigl, S. Lee, D.N. Schramm, and P. Coppi, *Phys. Lett.* **B392**, 129 (1997).

[27] S. Yoshida, G. Sigl, and S. Lee, *Phys. Rev. Lett.* **81**, 5505 (1998).

[28] P. Lipari, *Astropart. Phys.* **1**, 195 (1993).

[29] V.L. Ginzburg and S.I. Syrovatskii, The Origin of Cosmic Rays (Pergamon Press, Oxford, 1964), pp. 284.

[30] M.S. Longair, High Energy Astrophysics (Cambridge University Press, 1981), pp. 285.

[31] L.V. Volkova, G.T. Zatsepin, and L.A. Kuz'michev, *Sov. J. Nucl. Phys.* **29**, 645 (1979).

[32] S. Iyer Dutta, M.H. Reno, I. Sarcevic, and D. Seckel, *Phys. Rev.* **D63**, 094020 (2001).

[33] J. Jones, I. Mocioiu, M.H. Reno, and I. Sarcevic, *Phys. Rev.* **D69**, 033004 (2004).

[34] F. Becattini and S. Bottai, *Astropart. Phys.* **15**, 323 (2001).

[35] E. Bugaev et al., *Astropart. Phys.* **21**, 491 (2004).

[36] It should be noted that the X'-, X''-, and X'''-integration involving $\lambda_\tau^{\rm dec}$ in (19) and (20) cannot a priori be performed analytically, because of the appearance of the Earth's density $\rho(X,\theta)$. It turns out, however, that the exact numerical integrations can be reproduced to within 1% by using the reasonable approximation [4] $\rho(X,\theta) \simeq \rho_{av}(\theta)$ with the averaged $\rho_{av}(\theta)$ being not explicitly dependent on X (thus one can drop the explicit X dependence in, for example, $\lambda_\tau^{\rm dec}(E,\, X',\, \theta') \simeq \lambda_\tau^{\rm dec}(E,\, \theta)$ with $\theta' \equiv \theta(X') \simeq \theta(X) \equiv \theta$). Notice that $\rho_{av}(\theta) \equiv \int_0^L \rho\,(r(z,\theta))\; dz / \int_0^L dz = X(\theta)/L$ with $r(z,\theta) = \sqrt{R_\oplus^2 + z^2 - zL}$ and $L = 2R_\oplus \cos\theta$ (see, e.g., [15]). In particular the X''–integral in (20) receives its dominant contribution only from X'' being close to the upper limit of integration, $X'' \simeq X'$. Therefore the X'''–integral in (20) can be performed analytically. It should be furthermore noted that, when (20) is inserted into (19), $\lambda_\tau^{\rm dec}(E, X')$ in (19) gets cancelled to within a very good approximation (cf. Eq. (21)).

[37] P. Lipari and T. Stanev, *Phys. Rev.* **D44**, 3543 (1991).

[38] D. Chirkin and W. Rhode, hep–ph/0407075 (unpublished), and private communication.

[39] D. Fargion, astro–ph/9704205 (unpublished).

[40] D.E. Groom et al., Particle Data Group, *Phys. Lett.* **B592**, 1 (2004).

[41] R. Gandhi et al., *Phys. Rev.* **D58**, 093009 (1998).

[42] J.G. Learned and K. Mannheim, *Annu. Rev. Nucl. Part. Sci.* **50**, 679 (2000).

Table 1: Total nadir–angle–integrated upward–going $\mu^- + \mu^+$ event rates per year from $(\nu_\tau + \bar{\nu}_\tau)N$ and $(\nu_\mu + \bar{\nu}_\mu)N$ interactions in rock, with the latter being given in parentheses which are taken from Table 1 of [5], for various muon energy thresholds $E_\mu^{\rm min}$ and the appropriate dominant cosmic neutrino fluxes in Fig. 1. The $\nu_\tau + \bar{\nu}_\tau$ and $\tau^- + \tau^+$ initiated rates are calculated according to Eqs. (12) and (14) of Ref. [13], which are added to the $\nu_\mu + \bar{\nu}_\mu$ initiated rates in parentheses in order to obtain the final total rates. A bar signals that the rates fall below 0.01. This table corrects Table I of Ref. [13].

Flux	Detector	Muon-energy threshold $E_\mu^{\rm min}$/GeV				
		10^3	10^4	10^5	10^6	10^7
AGN-M95	ANTARES	16.63 (13.7)	6.28 (5.00)	2.51 (1.98)	1.06 (0.90)	0.34 (0.32)
	AMANDA-II	34.90 (29.1)	10.76 (8.62)	3.78 (2.98)	1.58 (1.34)	0.49 (0.46)
	IceCube	170.24 (143)	41.72 (33.7)	14.22 (11.2)	5.93 (5.04)	1.83 (1.74)
GRB-WB	ANTARES	0.75 (0.60)	0.39 (0.32)	0.10 (0.08)	0.01 (0.01)	—
	AMANDA-II	1.39 (1.10)	0.68 (0.56)	0.15 (0.13)	0.02 (0.02)	—
	IceCube	5.55 (4.35)	2.59 (2.13)	0.57 (0.49)	0.07 (0.06)	—
TD-SLBY	ANTARES	0.84 (0.62)	0.59 (0.45)	0.33 (0.26)	0.14 (0.12)	0.05 (0.05)
	AMANDA-II	1.33 (0.97)	0.91 (0.68)	0.49 (0.39)	0.21 (0.18)	0.07 (0.07)
	IceCube	5.11 (3.70)	3.42 (2.57)	1.84 (1.47)	0.78 (0.68)	0.26 (0.25)

Table 2: Nadir–angle–integrated upward–going $\mu^- + \mu^+$ event rates per year for muons with energy above $E_\mu^{\rm min} = 10^4$ GeV. The events produced by the primary $\nu_\mu + \bar\nu_\mu$, $\nu_\tau + \bar\nu_\tau$ and $\tau^- + \tau^+$ fluxes are given in parentheses, which are obtained from appropriately integrating the relevant dashed–dotted curves in Fig. 20. Notice that the total ($0^{\rm o} \leq \theta \leq 90^{\rm o}$) event rates in brackets in the last column agree of course with the final total rates in Table 1. Adding to these conventional primary rates the ones induced by the secondary $\nu_\mu + \bar\nu_\mu$ fluxes, originating from $\tau^+ \to \nu_\mu$ and $\tau^- \to \bar\nu_\mu$, one obtains the final results shown. These additional secondary $\nu_\mu + \bar\nu_\mu$ contributions are calculated according to (39) and correspond to integrating appropriately the relevant solid curves in Fig. 20.

Flux	Detector	Number of events			
		$0^\circ \leq \theta \leq 30^\circ$	$30^\circ \leq \theta \leq 60^\circ$	$60^\circ \leq \theta \leq 90^\circ$	Total
AGN-M95	ANTARES	0.19 (0.18)	1.13 (1.05)	5.25 (5.04)	6.58 (6.28)
	AMANDA-II	0.40 (0.38)	2.15 (2.03)	8.66 (8.34)	11.22 (10.76)
	IceCube	1.62 (1.54)	8.54 (8.06)	33.35 (32.13)	43.50 (41.72)
GRB-WB	ANTARES	0.02 (0.01)	0.10 (0.09)	0.28 (0.28)	0.39 (0.39)
	AMANDA-II	0.03 (0.03)	0.18 (0.17)	0.48 (0.48)	0.69 (0.68)
	IceCube	0.12 (0.11)	0.69 (0.67)	1.84 (1.82)	2.65 (2.59)
TD-SLBY	ANTARES	0.01 (0.01)	0.07 (0.06)	0.54 (0.52)	0.62 (0.59)
	AMANDA-II	0.01 (0.01)	0.12 (0.10)	0.83 (0.79)	0.96 (0.91)
	IceCube	0.05 (0.04)	0.44 (0.38)	3.14 (3.00)	3.63 (3.42)

Table 3: As in Table 2 but for $E_\mu^{\rm min} = 10^5$ GeV. A bar signals that the rates fall below 0.01.

Flux	Detector	Number of events			
		$0^\circ \leq \theta \leq 30^\circ$	$30^\circ \leq \theta \leq 60^\circ$	$60^\circ \leq \theta \leq 90^\circ$	Total
AGN-M95	ANTARES	0.01 (0.01)	0.20 (0.17)	2.46 (2.33)	2.67 (2.51)
	AMANDA-II	0.02 (0.02)	0.31 (0.26)	3.68 (3.50)	4.01 (3.78)
	IceCube	0.08 (0.06)	1.16 (0.98)	13.89 (13.20)	15.11 (14.22)
GRB-WB	ANTARES	—	0.02 (0.02)	0.08 (0.08)	0.10 (0.10)
	AMANDA-II	—	0.03 (0.03)	0.12 (0.12)	0.15 (0.15)
	IceCube	0.01 (0.01)	0.11 (0.10)	0.47 (0.46)	0.58 (0.57)
TD-SLBY	ANTARES	—	0.03 (0.02)	0.32 (0.30)	0.34 (0.33)
	AMANDA-II	—	0.04 (0.03)	0.48 (0.45)	0.52 (0.49)
	IceCube	0.01 (0.01)	0.14 (0.12)	1.79 (1.71)	1.94 (1.84)

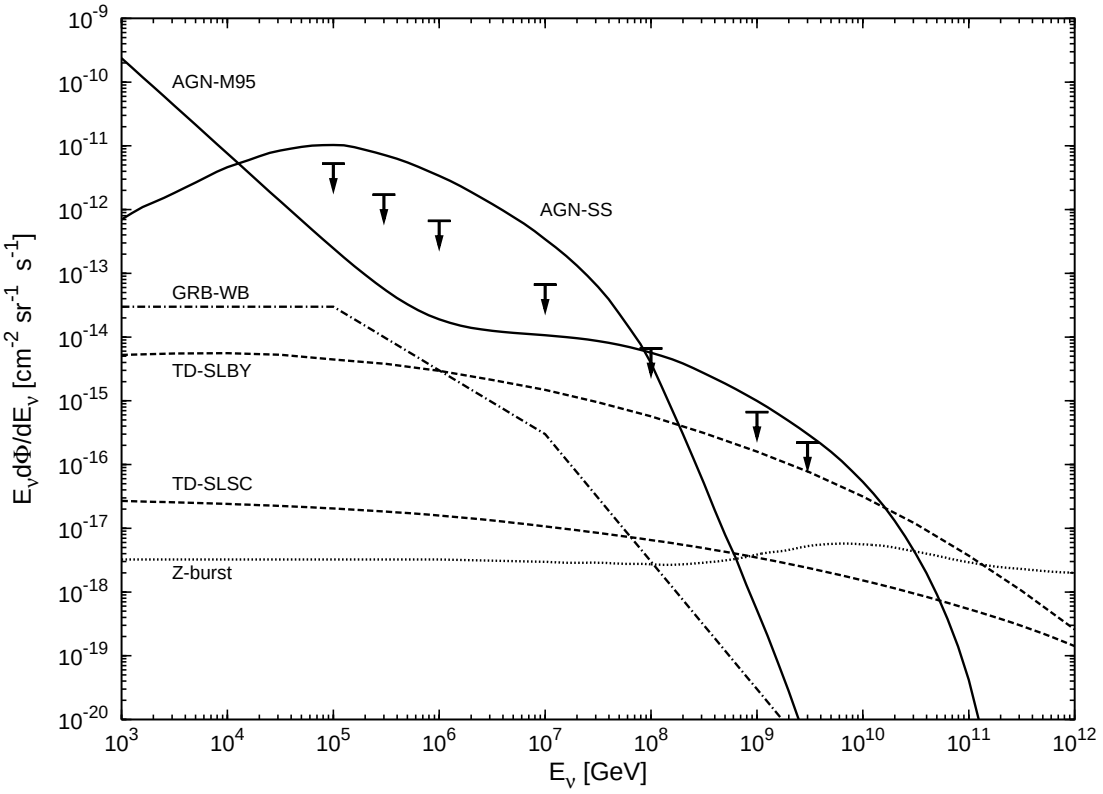

Figure 1: Representative differential fluxes of muon neutrinos ($\nu_\mu + \bar{\nu}_\mu$) at the production site from active galactic nuclei (AGN–SS [22] and AGN–M95 [23]), gamma ray bursts (GRW-WB [24]), toplogical defects (TD–SLBY [25] and TD–SLSC [26]) and Z–bursts [27]. Due to naive channel counting in pion production and decay at the production site ($\nu_e : \nu_\mu : \nu_\tau = 1 : 2 : 0$) and maximal mixing, $\nu_e : \nu_\mu : \nu_\tau = 1 : 1 : 1$, these fluxes are divided equally between e–, μ– and τ–neutrinos when they reach the Earth's surface (i.e. will be divided by a factor of 2). The diffuse neutrino flux upper limit of AMANDA [20, 21] are shown by the bars with arrows.

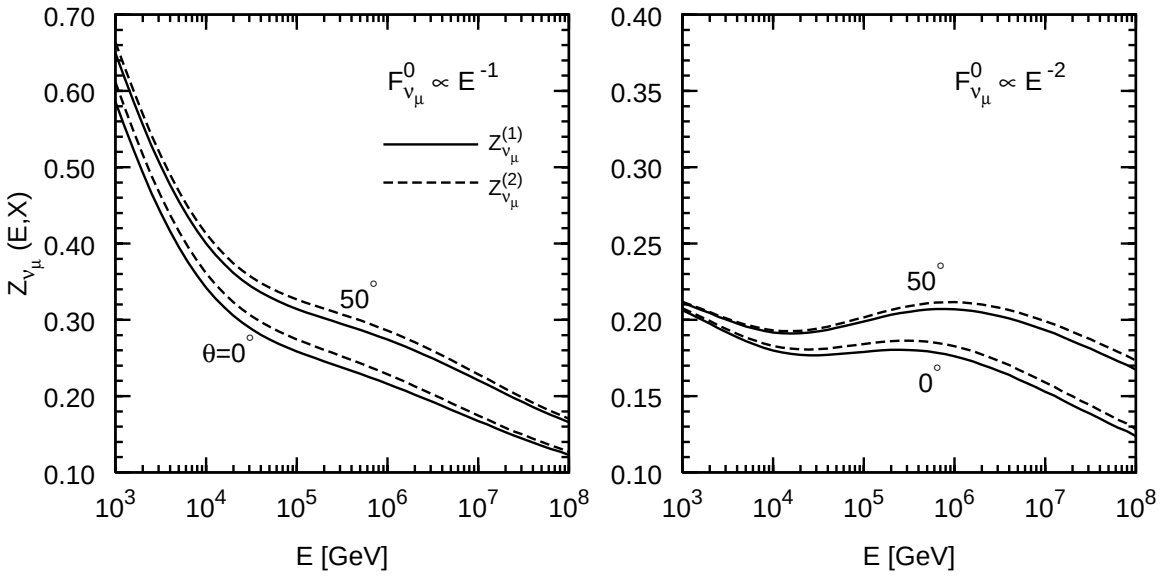

Figure 2: The Z_ν–factors for ν_μ neutrinos, as iteratively calculated according to (6), for the generic initial neutrino fluxes in (10) and (11) divided by 2. The result for the first order iteration $Z^{(1)}_{\nu_\mu}$ is given in (8). For nadir angles $\theta > 50^o$, the second order iterative result $Z^{(2)}_{\nu_\mu}$ becomes almost indistinguishable from $Z^{(1)}_{\nu_\mu}$.

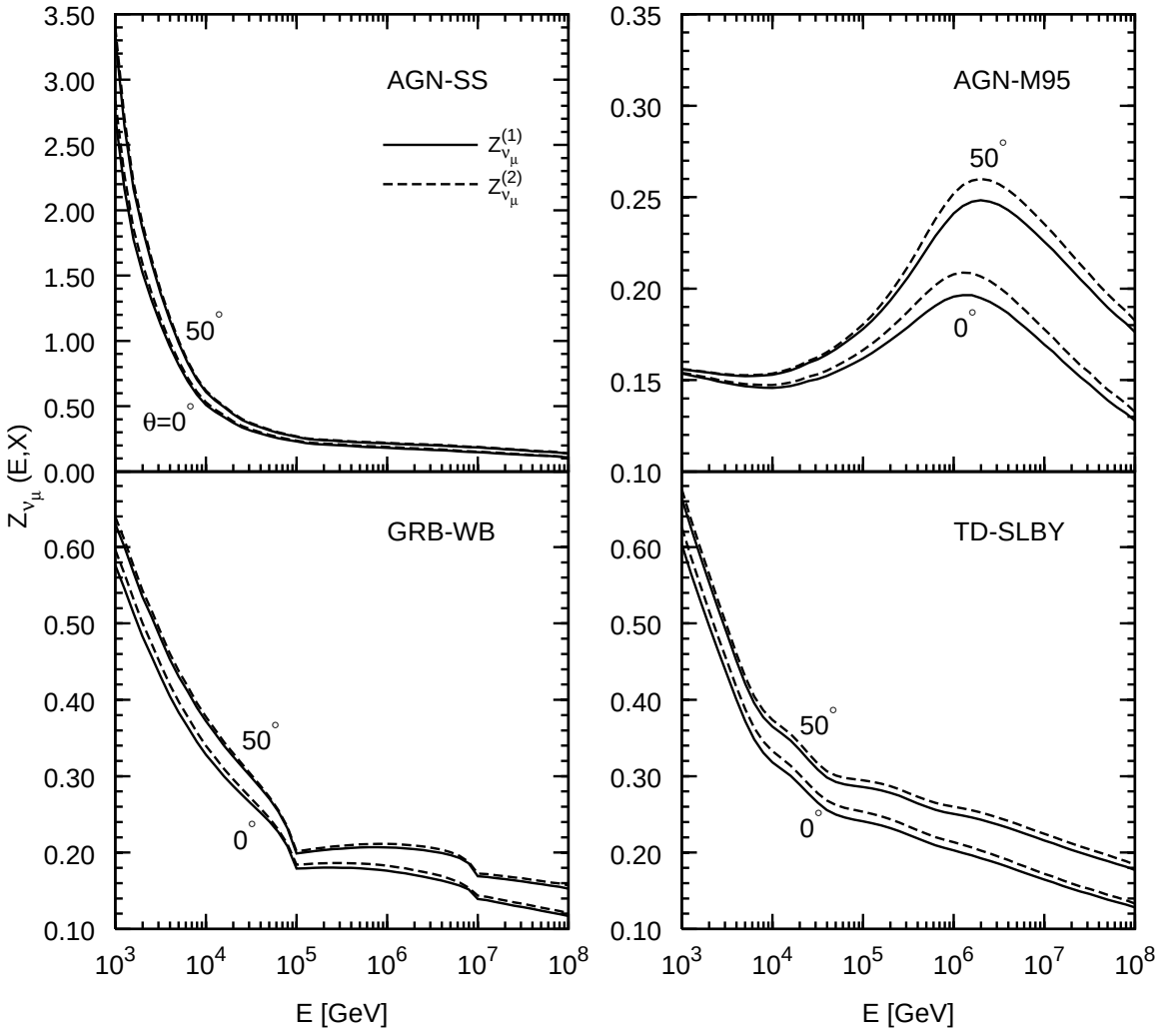

Figure 3: As in Fig. 2 but for some typical initial cosmic fluxes shown in Fig. 1. The (small) TD–SLSC and Z–burst fluxes in Fig. 1 result in a similar iterative convergence as the $F^0_{\nu_\mu} \sim E^{-1}$ flux in Fig. 2.

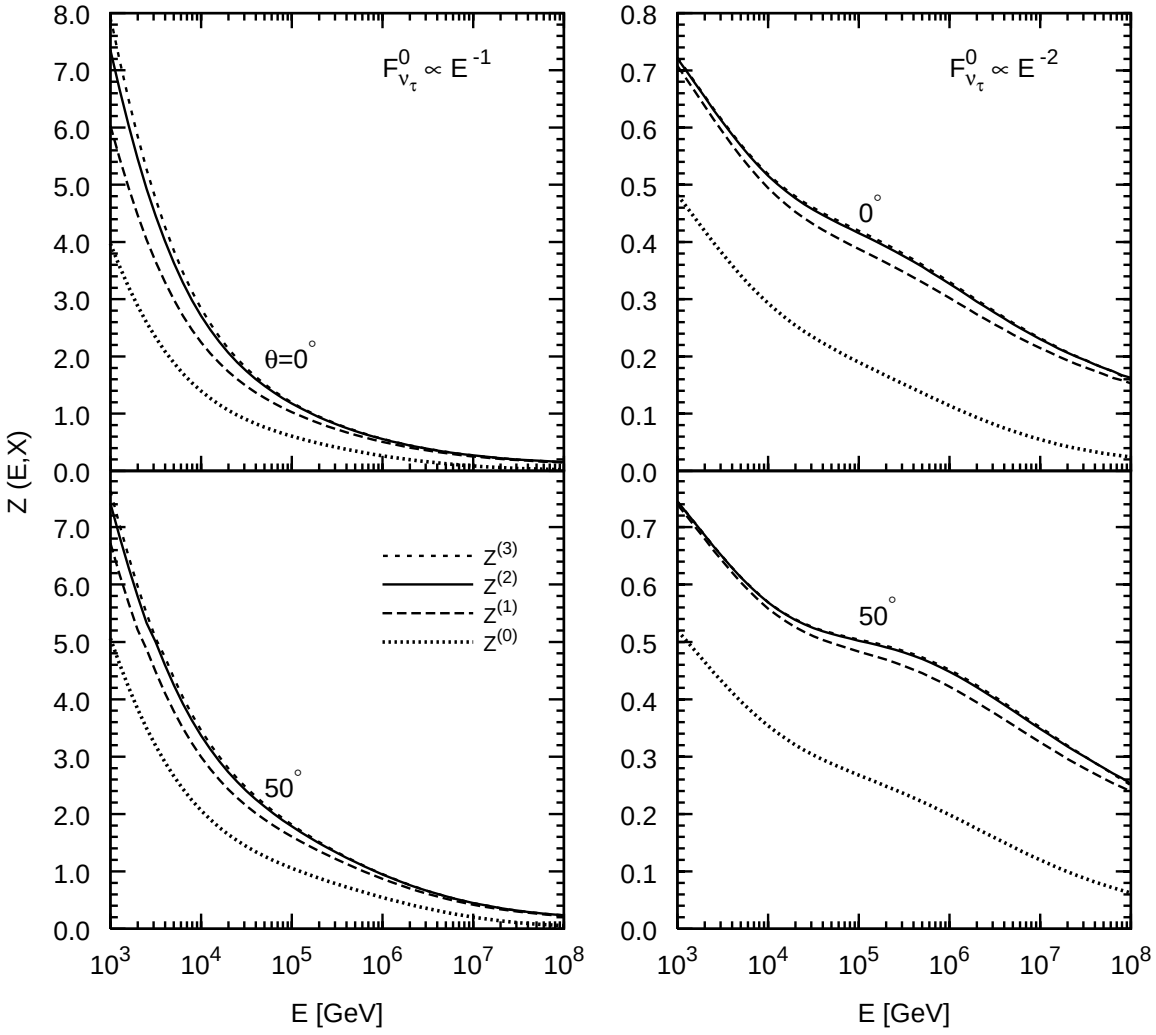

Figure 4: The Z–factors for ν_τ neutrinos, $Z^{(n)} = Z^{(n)}_{\nu_\tau} + Z^{(n)}_{\tau^-}$, as iteratively calculated for $n = 1, 2, 3$ iterations using the input $Z^{(0)}$ of (21) which is shown by the dotted curves. The generic initial fluxes are taken from (10) and (11) divided by 2.

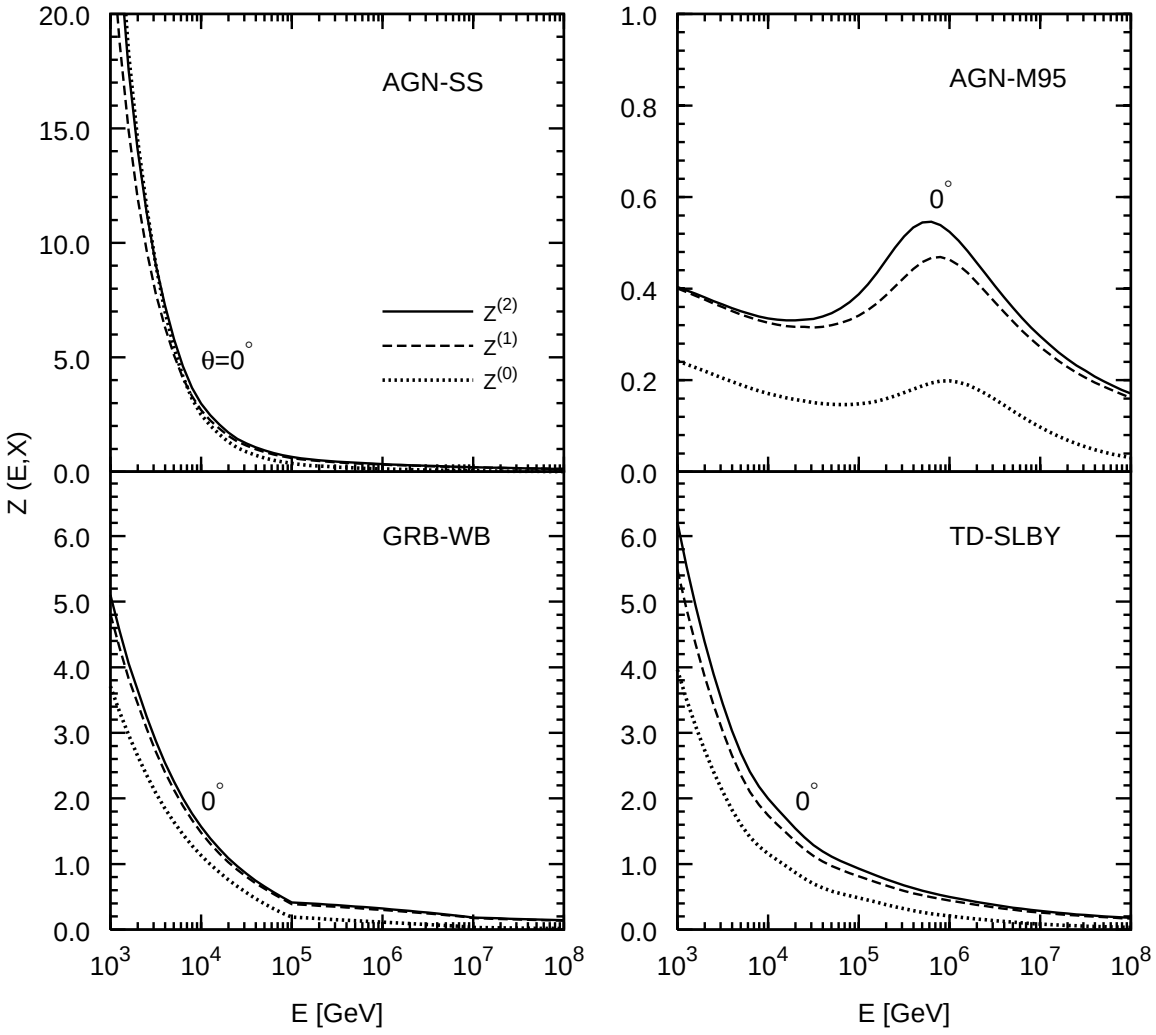

Figure 5: As in Fig. 4 but only for the relevant $n = 1$, 2 iterations for $\theta = 0^{\rm o}$ and for the dominant initial cosmic fluxes in Fig. 1.

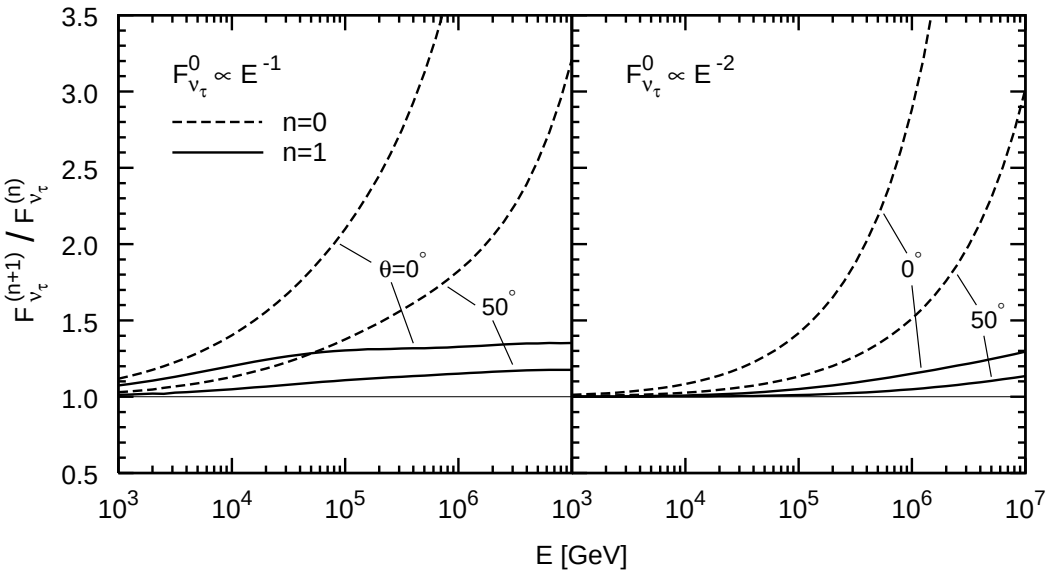

Figure 6: The ratios of the ν_τ fluxes $F^{(n+1)}_{\nu_\tau}/F^{(n)}_{\nu_\tau}$ according to two consecutive iterations. The fluxes are calculated according to (24) using the appropriate $Z^{(n)}$ factors shown in Fig. 4 for the two generic E^{-1} and E^{-2} initial fluxes.

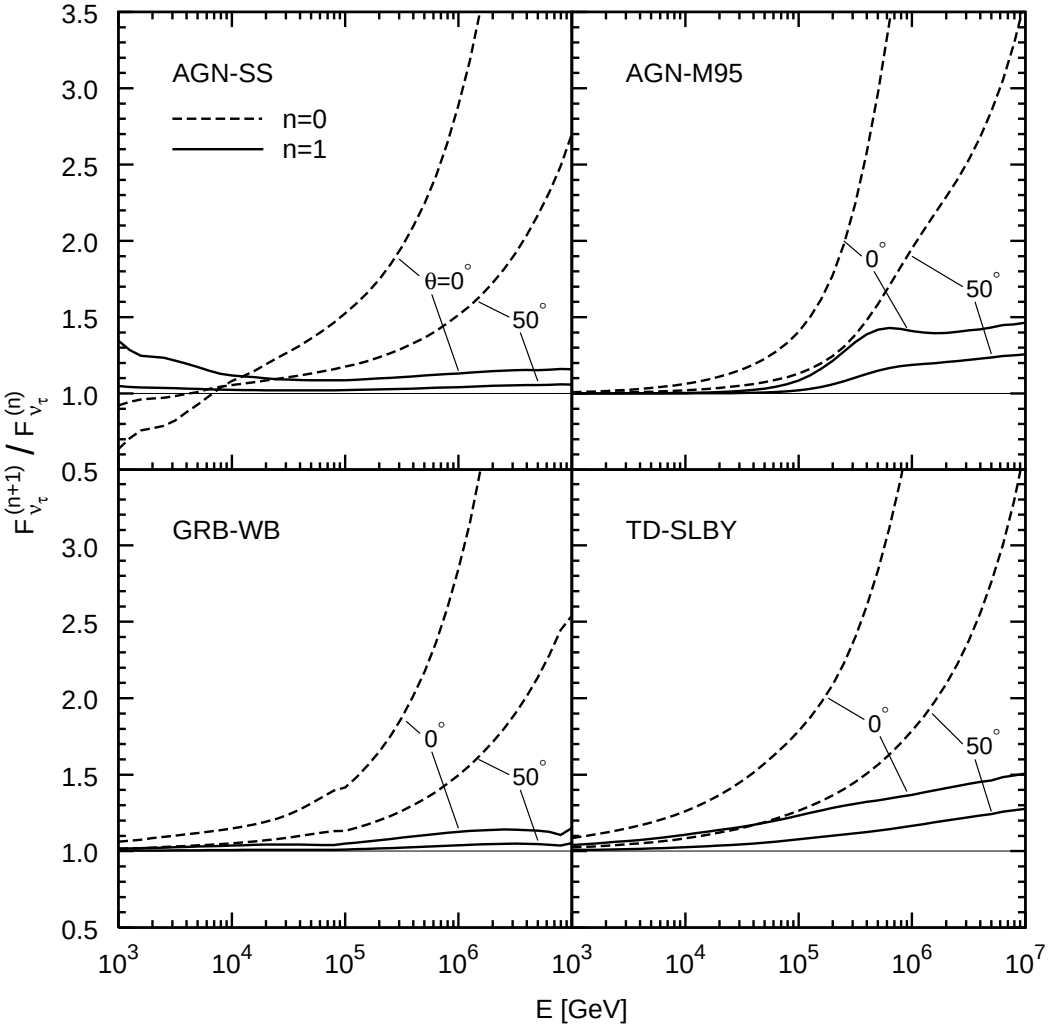

Figure 7: As in Fig. 6 but with the appropriate $Z^{(n)}$ factors shown in Fig. 5 as obtained for the dominant initial cosmic fluxes in Fig. 1.

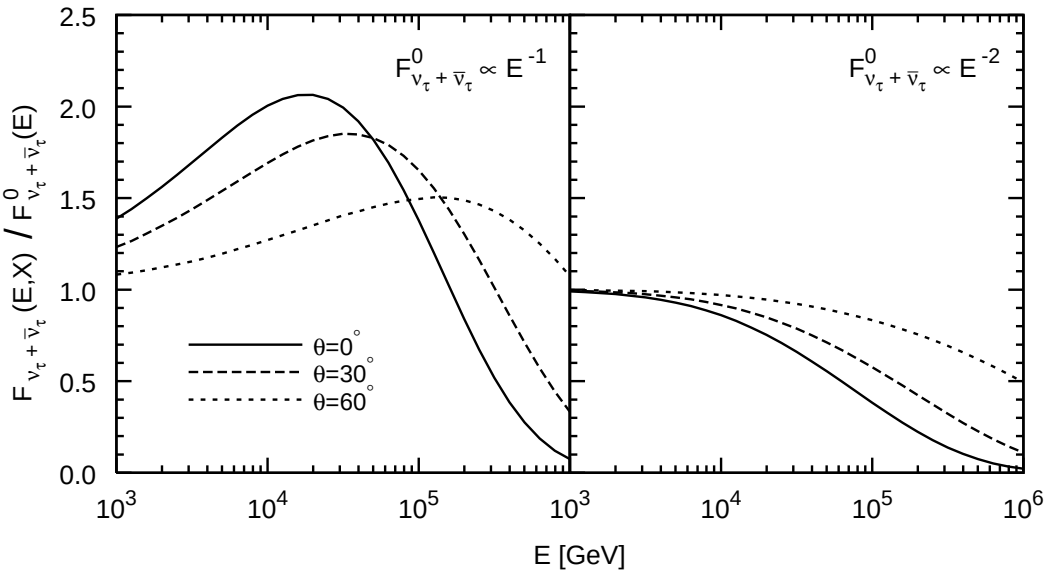

Figure 8: The final total $\nu_\tau + \bar{\nu}_\tau$ fluxes, calculated according to (24) using the appropriate iterative $n = 2$ results $Z^{(2)}$ for $\theta = 0^o$, 30^o and 60^o ($Z^{(2)}$ for $\theta = 0^o$ is shown in Fig. 4). The generic initial fluxes $F^0_{\nu_\tau + \bar{\nu}_\tau}(E)$ are given in (10) and (11).

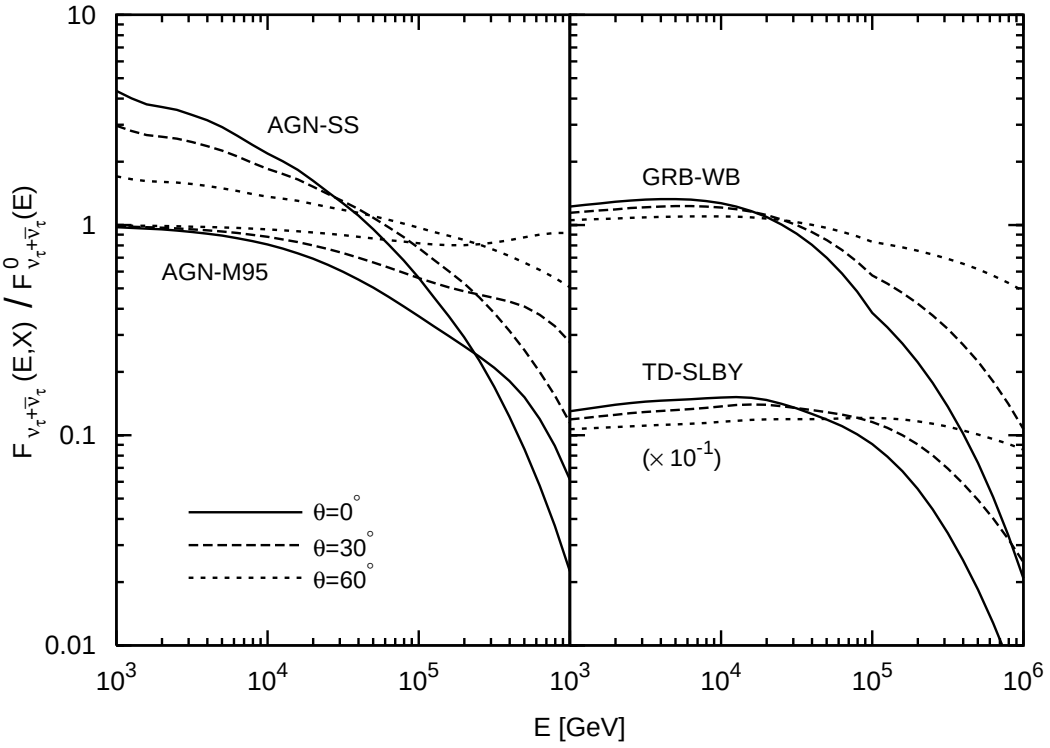

Figure 9: As in Fig. 8 but for the dominant initial cosmic fluxes $F^0_{\nu_\tau+\bar{\nu}_\tau}(E)$ in Fig. 1. For $\theta = 0^o$ the relevant $Z^{(2)}$ factors are shown in Fig. 5. The TD–SLBY results are multiplied by 10^{-1} as indicated.

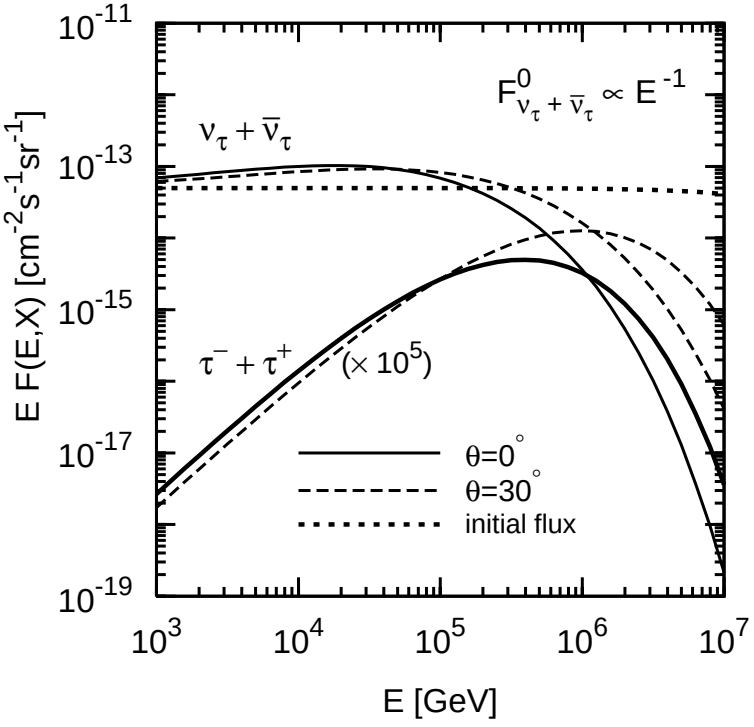

Figure 10: Attenuated and regenerated $\nu_\tau + \bar{\nu}_\tau$ and $\tau^- + \tau^+$ fluxes calculated according to (24) and (25), respectively, using the sufficiently accurate second iterative solution $Z^{(2)}(E, X)$ for nadir angles $\theta = 0^o$ and 30^o, and the generic initial $F^0_{\nu_\tau + \bar{\nu}_\tau}(E)$ flux in (10) which is shown by the dotted curve. The results for the $\tau^- + \tau^+$ fluxes are multiplied by 10^5 as indicated.

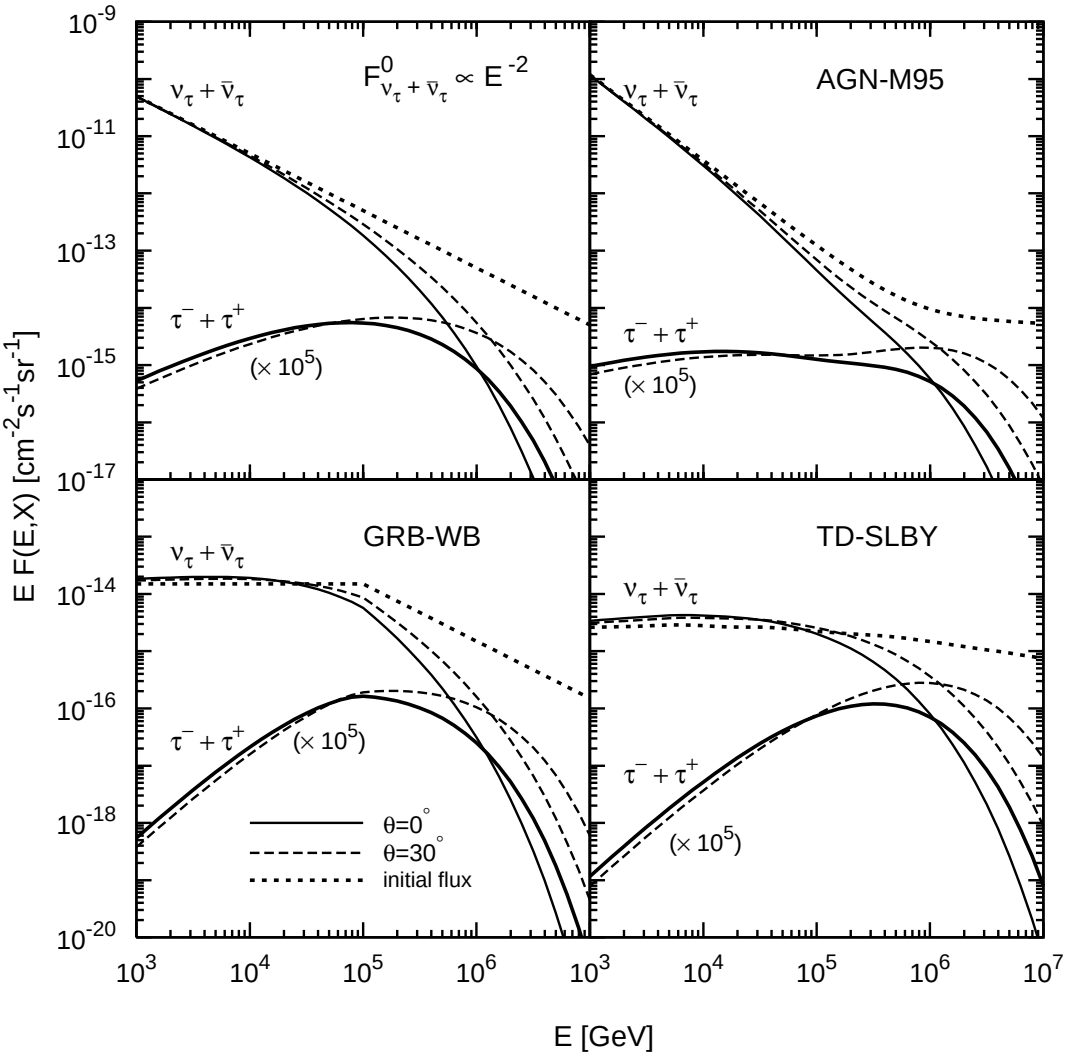

Figure 11: As in Fig. 10 but for the generic E^{-2} flux in (11) and the relevant dominant initial fluxes $F^0_{\nu_\tau+\bar\nu_\tau} = \frac{1}{2}\, d\Phi/dE_\nu$ in Fig. 1 which are shown by the dotted curves.

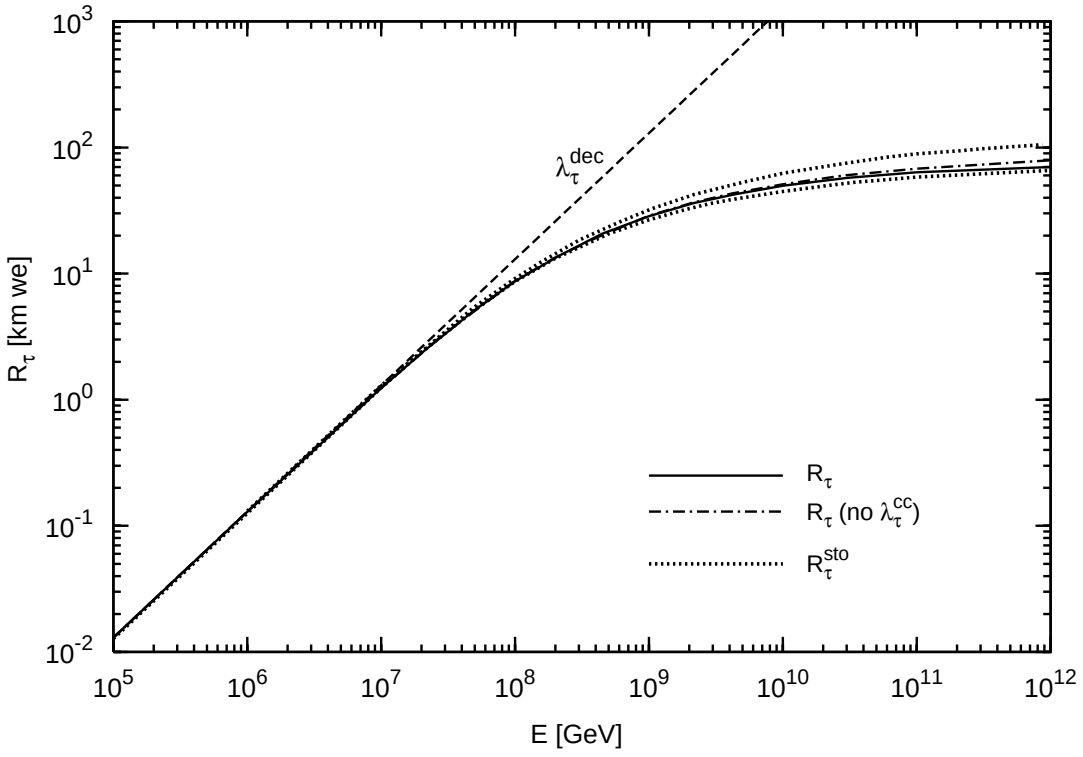

Figure 12: The τ–decay length $\lambda_\tau^{\rm dec} = (E/m_\tau)c\tau_\tau\rho$, shown by the dashed curve, and the τ–ranges in standard rock ($\rho = 2.65$ g/cm^3) for an incident τ–energy E and final τ–energy larger than $E^{\rm min} = 50$ GeV. R_τ is calculated according to (27) and (28); omitting $\lambda_\tau^{\rm CC}$ in (27) results in R_τ(no $\lambda_\tau^{\rm CC}$). The stochastic Monte Carlo evaluations of $R_\tau^{\rm sto}$ are shown by the upper dotted curve [38] and the lower one according to [32, 35] which are based on the ALLM97 parametrization of structure functions for calculating the photonuclear cross section. Using a different parametrization (Bugaev–Schlepin) for extrapolating the latter cross section to ultrahigh energies, results in a τ–range which is about 25% smaller than the upper dotted curve at $E = 10^{12}$ GeV [38].

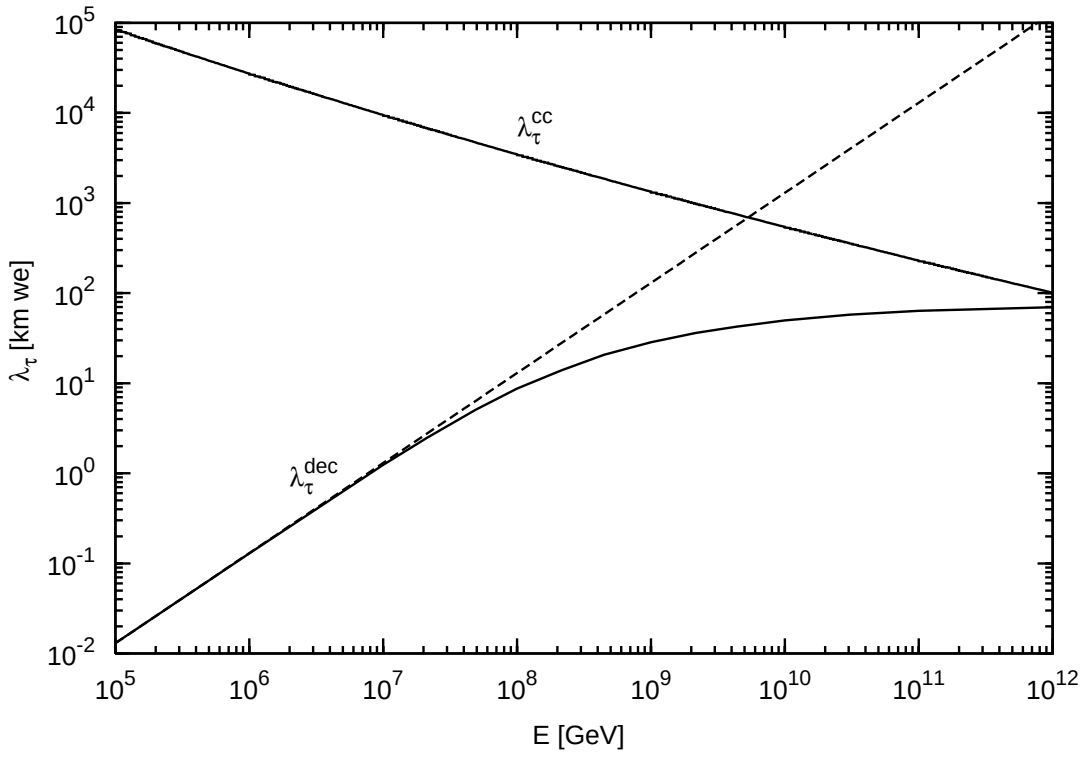

Figure 13: The CC τ–interaction length $\lambda_\tau^{\rm CC}$ (upper solid curve) and the τ–decay length neglecting the energy–loss (dashed curve) and including the energy–loss in standard rock (lower solid line). The latter two curves correspond to the ones shown in Fig. 12.

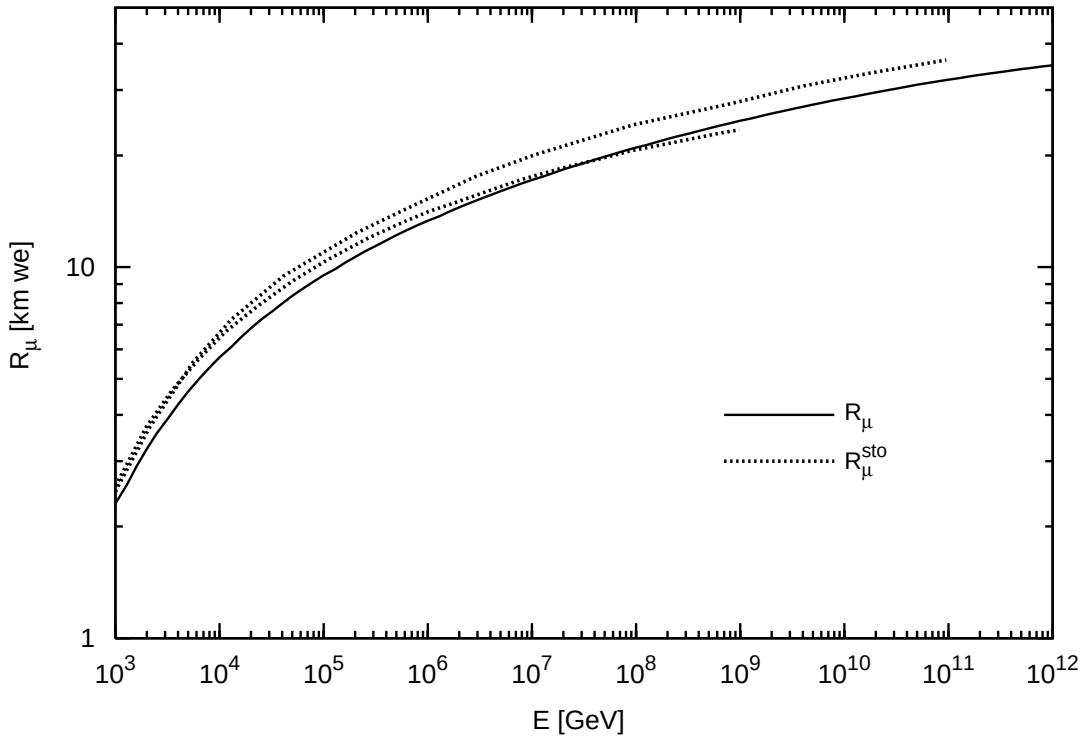

Figure 14: The μ–ranges in standard rock ($\rho = 2.65$ g/cm^3) for an incident muon energy E and the final μ–energy larger than $E^{\min} = 1$ GeV. R_μ is calculated according to (27) and (28) as discussed in the text. The stochastic Monte Carlo evaluations of $R_\mu^{\rm sto}$ are taken from [32, 35] (lower dotted curve) and from [38] (upper dotted curve).

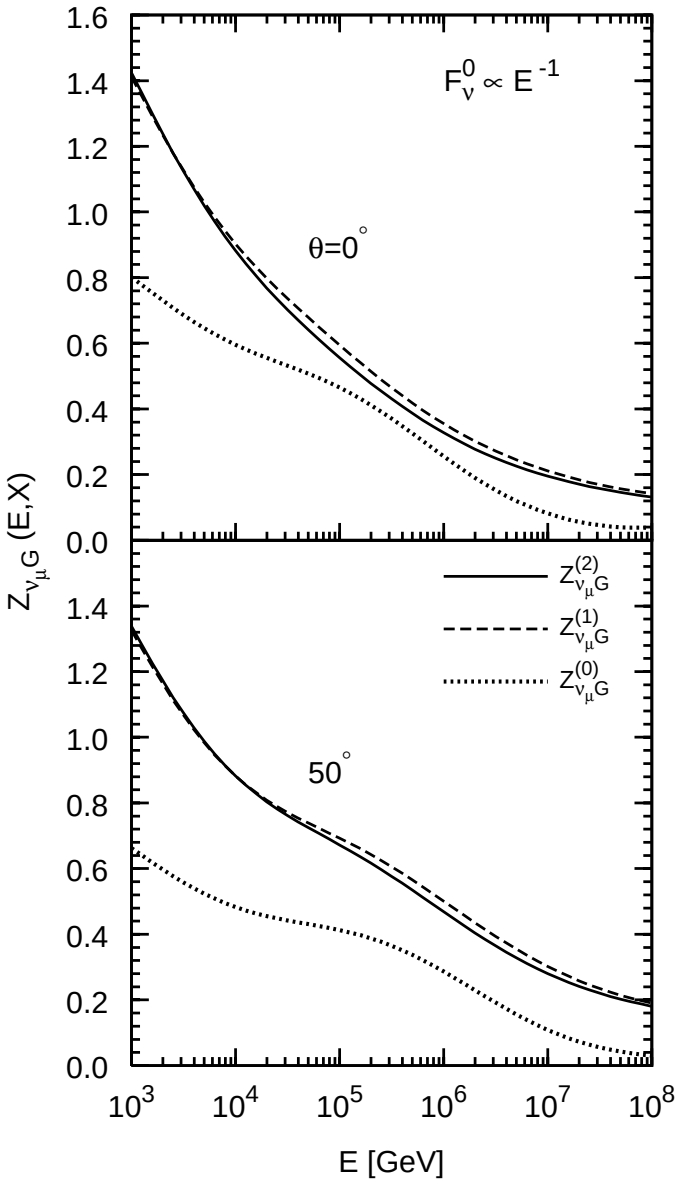

Figure 15: The Z–factors for primary and secondary ν_μ neutrinos, $Z^{(n)}_{\nu_\mu G} = Z^{(n)}_{\nu_\mu} + Z^{(n)}_G$, as defined in (34), (35), (36) and calculated iteratively for $n = 1$, 2 according to (37) using the input $Z^{(0)}_{\nu_\mu G}$ of (38) which is shown by the dotted curves. The generic initial E^{-1} flux is taken from (10) divided by 2.

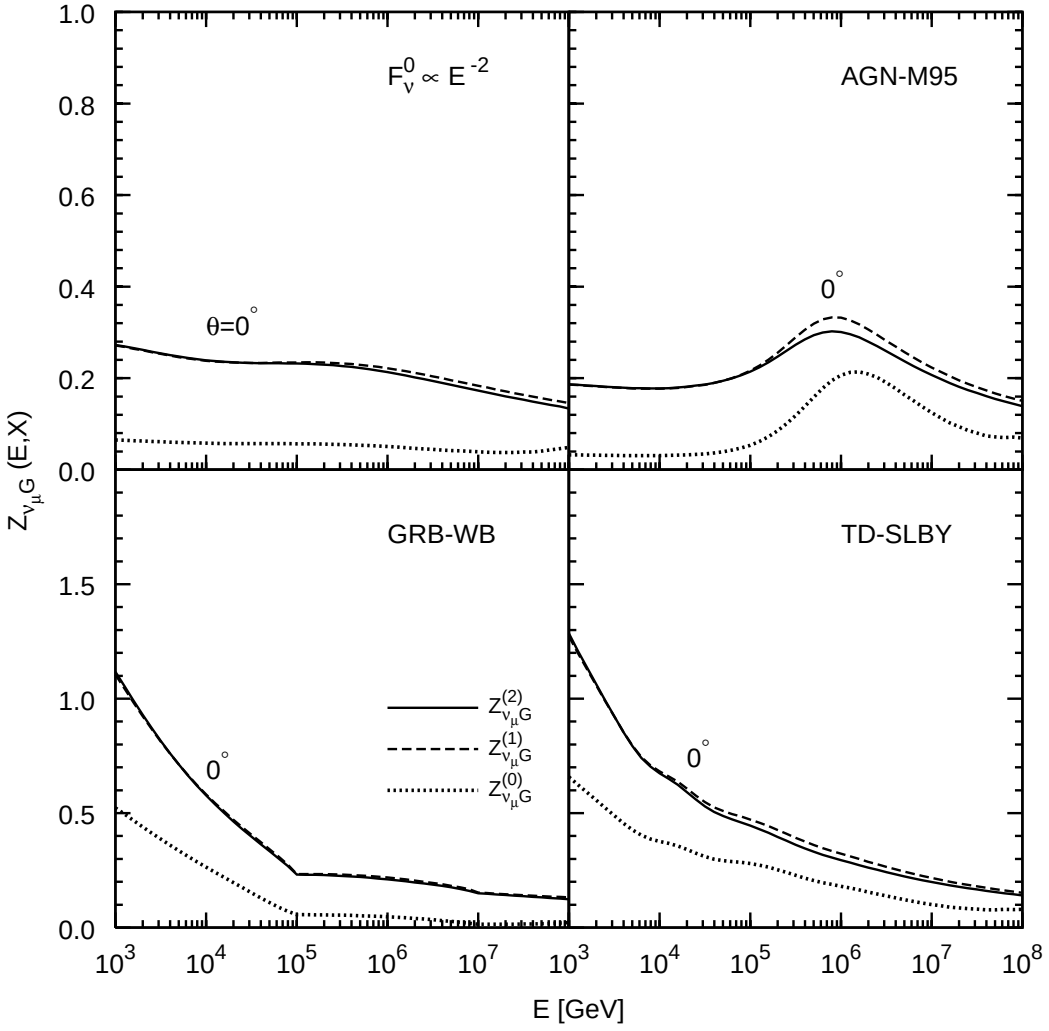

Figure 16: As in Fig. 15 but only for $\theta = 0^o$ and for the generic initial E^{-2} flux in (11), divided by 2, and the three dominant initial cosmic fluxes in Fig. 1.

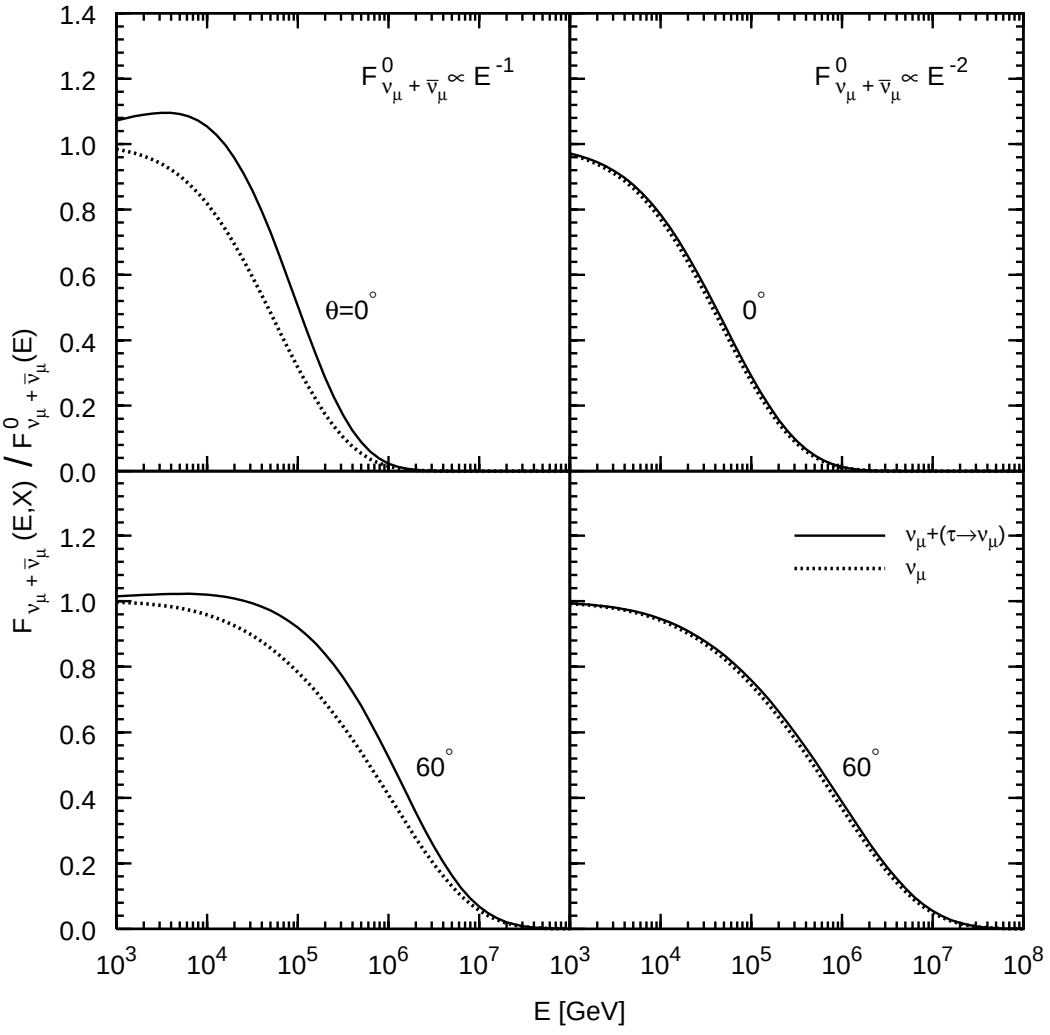

Figure 17: The final total $\nu_\mu + \bar\nu_\mu$ fluxes for primary and secondary muon neutrinos, calculated according to (33) using the appropriate iterative $n = 2$ results for $Z^{(2)}_{\nu_\mu G}$ for $\theta = 0^o$ and 60^o. The generic initial fluxes $F^0_{\nu_\mu+\bar\nu_\mu}(E)$ are given in (10) and (11). The usual primary $\nu_\mu + \bar\nu_\mu$ fluxes are for brevity denoted by ν_μ (dotted curves). Similarly the secondary neutrino contributions due $\tau^+ \to \nu_\mu$ and $\tau^- \to \bar\nu_\mu$ are denoted by $\tau \to \nu_\mu$.

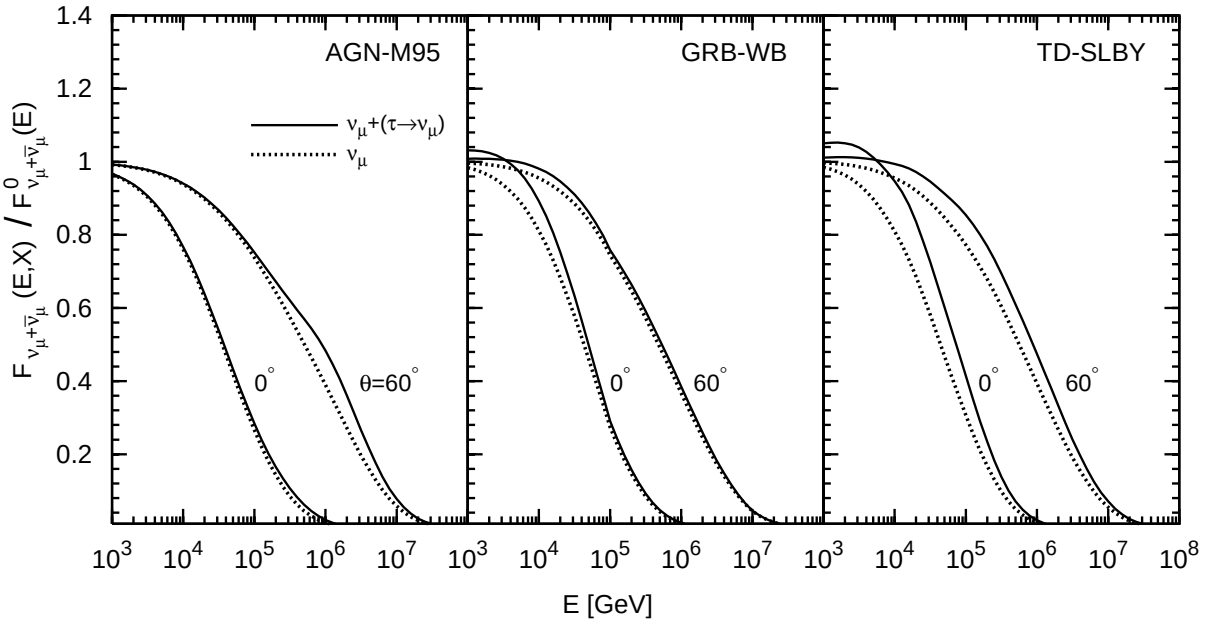

Figure 18: As in Fig. 17 but for the three dominant initial cosmic fluxes $F^0_{\nu_\mu+\bar{\nu}_\mu}(E)$ in Fig. 1.

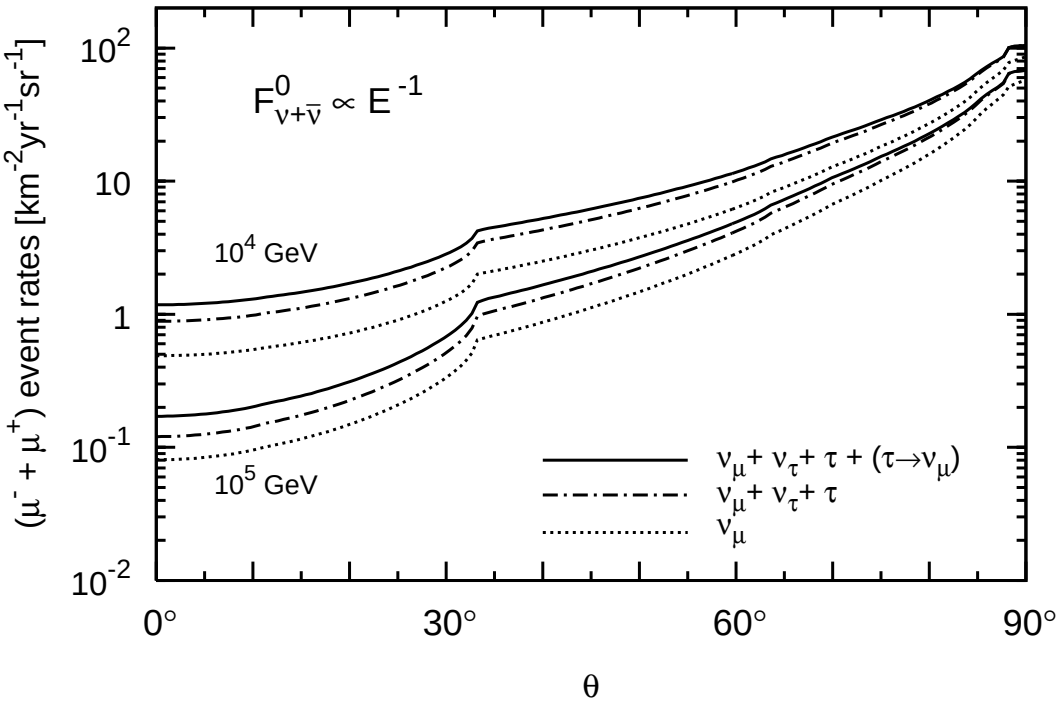

Figure 19: The $\mu^- + \mu^+$ event rates for muons with energy above 10^4 and 10^5 GeV originating from (anti)neutrinos with $E_\nu \leq 10^8$ GeV for the generic initial E^{-1} flux in (10). The muon events initiated by the primary $(\nu_\mu + \bar{\nu}_\mu)$ and $(\nu_\mu + \bar{\nu}_\mu) + (\nu_\tau + \bar{\nu}_\tau) + (\tau^- + \tau^+)$ fluxes are for simplicity denoted by ν_μ and $\nu_\mu + \nu_\tau + \tau$, respectively (dotted and dashed–dotted curves). The additional events initiated by the secondary muon neutrinos arising from $\tau^- \to \bar{\nu}_\mu$, $\tau^+ \to \nu_\mu$ are for brevity denoted by $(\tau \to \nu_\mu)$.

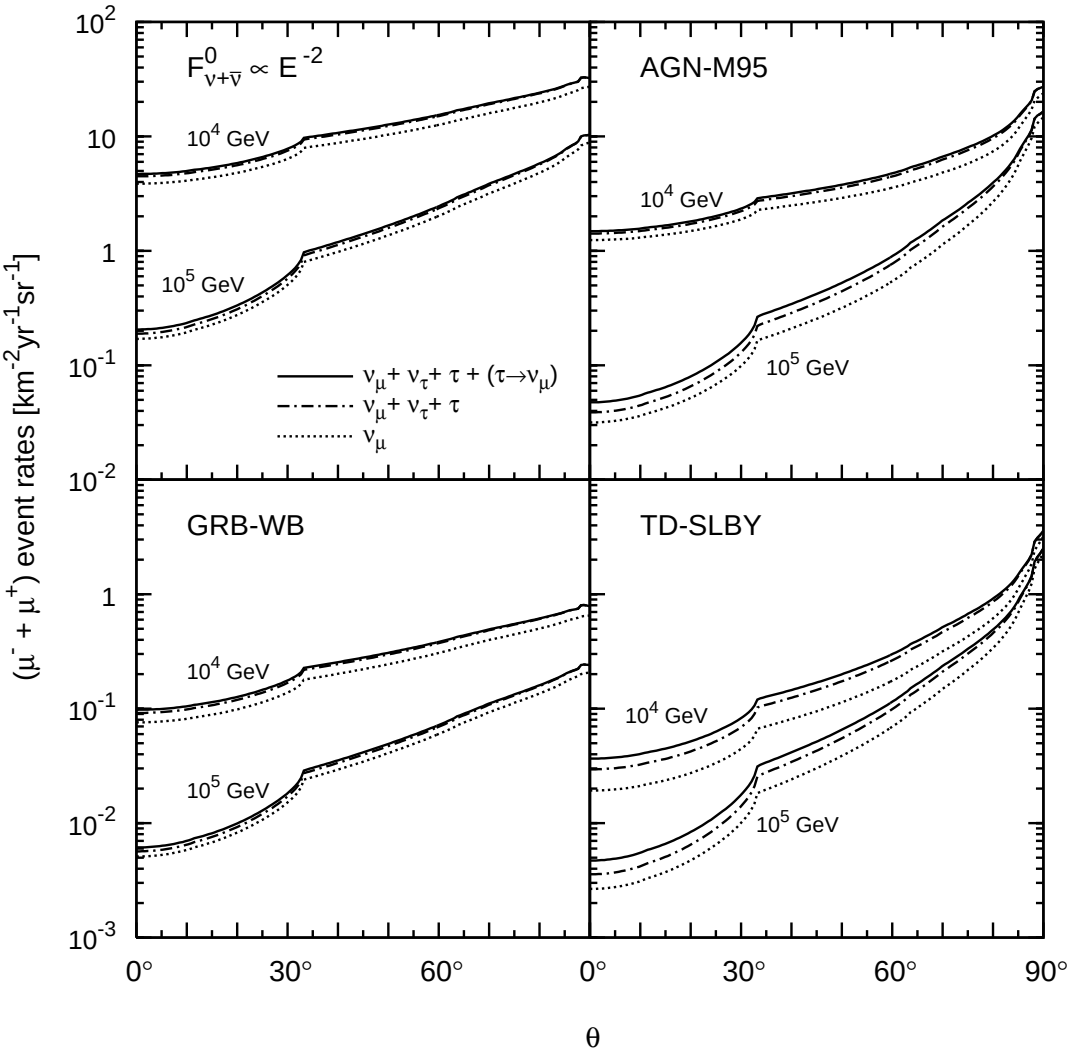

Figure 20: As in Fig. 19 but for the generic initial E^{-2} flux in (11) and for the three dominant initial cosmic fluxes in Fig. 1.